

Transformation of orientation and rotation angles of synchronous satellites: Application to the Galilean moons

Marie Yseboodt and Rose-Marie Baland
 Royal Observatory of Belgium, m.yseboodt@oma.be,
 Avenue Circulaire 3, Brussels, Belgium

December 8, 2025

Highlights

- We define the analytical transformation between Laplace plane and ICRF systems.
- We propose an updated orientation/rotation solution, based on a non-zero obliquity model.
- Second-order terms ensure transformation accuracy in the order of arcseconds.
- The transformation preserves the trigonometric form of the series.

Abstract

The orientation and rotation of a synchronous satellite can be referred to both its Laplace plane and the ICRF equatorial plane, in terms of Euler angles or spin axis Cartesian coordinates and Earth equatorial coordinates, respectively. We computed second-order analytical expressions to make the transformation between the two systems and applied them to the Galilean satellites (Io, Europa, Ganymede, and Callisto). If one term of the spin axis Cartesian coordinates series is dominant, trigonometric series can be generated for the inertial and orbital obliquities, node longitude and offset with respect to the Cassini plane. Since the transformation does not require any fit of amplitudes and frequencies on numerical series, the physical meaning of the frequencies is preserved from the input series and the amplitudes can be directly related to the geophysical parameters of interest. We provide tables for the coordinates and angles' series assuming that the satellites are entirely solid, and considering two different orbital theories. The possible amplitude ranges for the main terms are also examined in the case where a liquid layer is assumed in the interior model. We use our transformation method to propose an updated IAU WG solution which would result in an improvement with respect to zero obliquity models used so far. This method will also be useful for the interpretation of future Earth-based radar observations or JUICE data.

Icarus Keywords: Rotational dynamics; Satellites, dynamics; Jupiter, satellites

1 Introduction

The synchronous rotation of the Jupiter's Galilean satellites, Io, Europa, Ganymede, and Callisto, was only confirmed with certainty after decades of observations of their surface features from Earth telescopes, see Camichel et al. [1943], Dollfus and Murray [1974].

The Galilean satellites are assumed to be in the so-called Cassini state [Colombo, 1966, Peale, 1969], which means that their rotation axis follows the long-term precession of their orbit normal while their rotation about the spin axis is periodically modified by physical libration, due to the torque exerted on their triaxial shape by Jupiter. The derivation of control networks for the Galilean satellites from images taken by Voyager 1 and 2 and Galileo did not reveal any significant deviation between their spin and orbit axes

[Davies and Katayama, 1981, Davies et al., 1998]. The obliquity of the satellites, which is the angular separation of the rotation axis and the orbit normal, is therefore expected to be small.

The obliquity and the libration amplitude of Ganymede will be measured with exquisite precision by JUICE's 3GM experiment during the Ganymede orbital phase (0.2 and 0.4 arcsec, respectively, see Cappuccio et al. [2020]), slightly better than the expected accuracy with the GALA instrument (between 0.5 and 1.7 arcsec, see Steinbrügge et al. [2019]). The obliquity of Europa cannot be measured by 3GM due to the limited data provided by the close flyby, whereas the obliquity of Callisto can be determined to within $0.06^\circ - 0.3^\circ$ [Cappuccio et al., 2022].

The Europa Clipper spacecraft's radio science and camera instruments will measure the orientation of Europa spin axis [Mazarico et al., 2023, Turtle et al., 2024] with a precision of the order of 0.05° and 0.001° , respectively. In parallel with space missions, the radar speckle tracking observations from Goldstone Solar System Radar and Green Bank Telescope between 2011 and 2023 provided estimates of the orientation of Europa and Ganymede's rotation axis with an accuracy of 0.01° , Margot [2025]. Note that on Europa and Ganymede, at the equator, 1 arcsec = 8 m and 13 m, while $0.0001 \text{ deg} = 3 \text{ m}$ and 5 m, respectively.

To make the most of these measurements, the rotation models for the satellites must be accurate, both in their description of the link between observables and internal parameters and in the orbital model used. This precise modeling has been an ongoing effort within the rotation community for about 20 years (e.g., Henrard [2005], Bills [2005], Van Hoolst et al. [2008], Noyelles [2009], Rambaux et al. [2011], Baland et al. [2012], Van Hoolst et al. [2013], Baland et al. [2016], Coyette et al. [2025]) and has certainly not yet reached its conclusion.

The orientation and rotation of a body can be described using at least two different sets of angles. The first set is the Euler angles with respect to a fixed plane with the inertial obliquity θ , the node longitude ψ and the prime meridian location ϕ . This fixed plane can be the equatorial plane of the central planet at J2000 or, preferably, the Laplace plane. The second set of angles is the Earth equatorial coordinates with respect to the Earth equator at J2000 (= International Celestial Reference Frame ICRF equatorial plane): right ascension α , declination δ and prime meridian location W angle.

These coordinates are adopted by the IAU Working Group on Cartographic Coordinates and Rotational Elements (WGCCRE) to define a rotation model for the main solar system bodies, see Archinal et al. [2018].

The goal of this study is to find analytical expressions to transform the orientation angles of the Galilean satellites between the Laplace plane and the ICRF equatorial plane, correct up to the second order in small parameters like the spin axis obliquity. This transformation can be applied if the orbital obliquity is assumed to be equal to 0 (orbit normal = spin axis) or finite and given by a theoretical model or by observations. It is therefore an improvement over the zero obliquity model, see for example Stark et al. [2018]. The method does not require a fit of amplitudes and frequencies on a numerical time series and preserves the physical meaning of the frequencies when the input quantities are given as series. Our transformation model can be used to define the future IAU WG solution for the rotation and orientation using right ascension, declination, and prime meridian location, as predicted by a theoretical model for the spin orientation. The link between the geophysical parameters of interest and the Earth equatorial coordinates will therefore be more direct than that obtained with a fit to a numerical series. This study is also useful for the interpretation of future Earth based observation or JUICE data, and can be applied to other satellites in synchronous rotation like Titan or the Uranian satellites.

Recently Yseboodt et al. [2023] described an analytical method that converts the Martian Euler angles into right ascension/declination and reciprocally, but this method can not be applied without any change for different reasons. First, the node longitude of the Galilean satellites shows a large precession rate (periods of 7, 30, 130 and 560 years) while the Martian method works better for periodic motion with a small precession rate (period of about 26 ky for Mars). Therefore the precession term can be considered as a first-order quantity for Mars but not for the Galilean satellites.

Second, contrary to Mars obliquity ε that is about 25° , the obliquity of the Galilean satellites is very small, probably much smaller than 1° . The denominators of the Mars transformation coefficients are usually proportional to $\sin \varepsilon$, which may give approximate first-order coefficients with large value. Lastly, the spin Cartesian coordinates s_x and s_y projected onto the Laplace plane are easily expressed as trigonometric series computed from the orbital forcing series and therefore are better suited as a starting point than the Euler

angles θ and ψ for a transformation to Earth equatorial coordinates.

The paper is organized as follows. Section 2 defines the relevant planes and angles. Sections 3 and 4 present the transformation equations for the spin orientation and rotation angles, respectively. In Section 5, we introduce a dynamical model for a solid planet, which serves as the basis for generating multiple trigonometric series in Section 6. Section 7 provides recommendations for the IAU WGCCRE. Finally, Section 8 discusses the implications of adopting an alternative ephemerides and the effects of a potential liquid layer.

2 Planes and angles

The transformation of a position \vec{r} in the satellite body frame (BF) to its position in the Inertial Frame (IF) \vec{R} is:

$$\vec{R} = \mathbf{M} \vec{r}, \quad (1)$$

with \mathbf{M} the rotation matrix from the BF to the IF. The BF frame is attached to the satellite and centered at its center of mass. Its x and y -axes define the satellite's equator, and its z -axis defines its figure axis. Galilean satellites should experience polar motion due to the gravitational torque exerted by their parent planet [Coyette et al., 2025]. This is also the case for Titan, which in addition experiences polar motion due to the exchanges of angular momentum between a seasonally-varying atmosphere and the solid surface [Coyette et al., 2016, 2018]. However, for the sake of simplicity, we assume here that the figure axis coincides with the spin axis. Including polar motion in the transformation would simply require additional rotations, see for example Eqs. (1-3) of Yseboodt et al. [2023]. The IF is also centered at the center of mass, but its equatorial plane is the Earth mean equator at the J2000 reference epoch (or the equator of the International Celestial Reference Frame ICRF). The IF X -axis points towards the ascending node of the ecliptic on the Earth equator (i.e. towards the vernal point IE in Fig. 1). The transformation matrix \mathbf{M} can be written in two different ways:

$$\mathbf{M} = \mathbf{M}_{\theta\psi\phi} = R_Z\left(-\frac{\pi}{2} - \alpha_{LP}\right) \cdot R_X\left(-\frac{\pi}{2} + \delta_{LP}\right) \cdot R_Z(-\psi) \cdot R_X(-\theta) \cdot R_Z(-\phi), \quad (2a)$$

$$= \mathbf{M}_{\alpha\delta W} = R_Z\left(-\frac{\pi}{2} - \alpha_S\right) \cdot R_X\left(-\frac{\pi}{2} + \delta_S\right) \cdot R_Z(-W), \quad (2b)$$

depending on whether Euler (θ, ψ, ϕ) or Earth equatorial (α_S, δ_S, W) angles are used for the spin position.

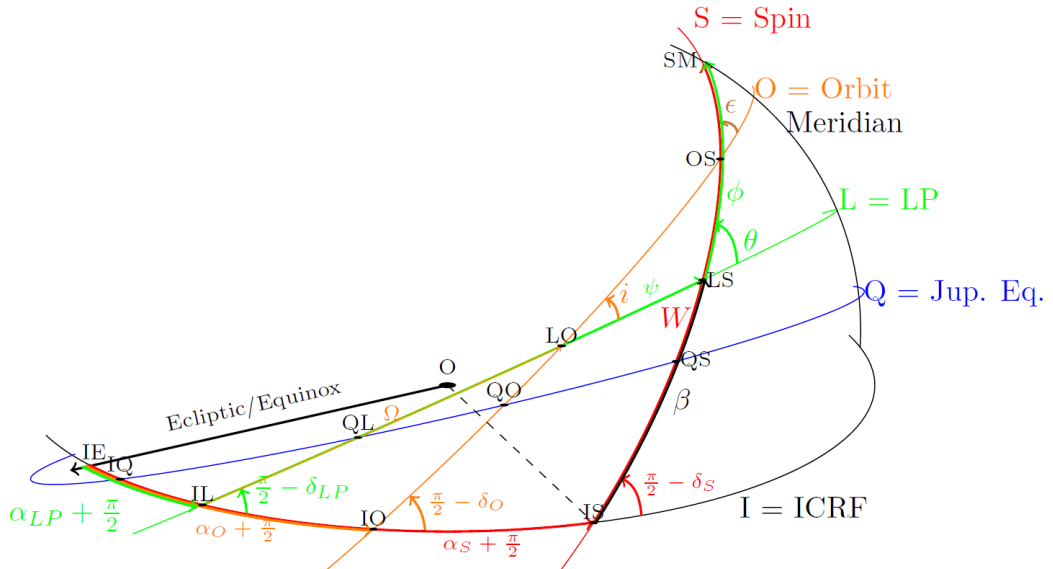


Figure 1: Planes and angles. Angles are not drawn to scale but are exaggerated for the purpose of illustration.

The orientation of the z -axis is either defined by the inertial obliquity θ and the node longitude ψ with respect to the Laplace plane, or either by the right ascension α_S and declination δ_S with respect to the ICRF. The Laplace plane (LP) is the mean plane around which the instantaneous orbital plane of the

satellite precesses, see Section 2.2. Note that here $\psi = \Omega_{ILLS}$ is the angle measured from the node of the Laplace plane on the ICRF, a convention that differs from that of Baland et al. [2012], where $\psi = \Omega_{QLLS}$ is measured from the node of the Laplace plane on the equator of Jupiter. The inertial obliquity θ of the spin axis is measured from the Laplace plane pole, and should not be confused with the orbital obliquity ε , measured from the orbit normal.

The prime meridian (x -axis of BF) is positioned by ϕ or W , depending on the angles' set, see Fig. 1. The difference $W - \phi$ is defined as the angle β , which varies with time, see Section 4. The rotation angle ϕ of the satellite must include periodic variations, called librations, with respect to synchronous rotation. These variations are also included in W .

The Earth equatorial angles, as adopted by the Cartographic Coordinates and Rotational Elements Working Group from the IAU, can be used for data analysis. Euler angles are, however, preferred by the rotation modeling community. Dynamical models for spin precession caused by the gravitational torque exerted on the satellite by the parent planet generally resolve the orientation of the satellite with respect to a reference plane, which is the orbit or the Laplace plane, whereas libration models resolve for the rotation variations with respect to synchronicity with the orbital motion (see Section 5).

We position the Laplace plane for each satellite in the ICRF frame with two angles that are constant over time: the right ascension α_{LP} and the declination δ_{LP} (see Fig. 1). $\Omega_{IEIL} = \alpha_{LP} + \pi/2$ is the node longitude along the ICRF equator from the ecliptic to the Laplace plane. $i_{IL} = \pi/2 - \delta_{LP}$ is the inclination of the Laplace plane on the ICRF equator. The orientation of the orbital plane is defined with i and Ω , the orbital inclination and longitude of the node with respect to the Laplace plane, or with α_O and δ_O , the orbital right ascension and declination with respect to the ICRF. Note that the position of the parent planet in a frame centered on the satellite, measured from the orbital node on the Laplace plane, is defined by the sum $\omega - \pi + f$, with ω and f the argument of the pericenter and the true anomaly, respectively, and by the semi-major axis a and eccentricity e .

2.1 The orbital theory

The four Galilean satellites form a complex dynamical system. Their orbital variations, including precession, are mainly driven by the planet's flattening on the one hand, and by mutual perturbations between the satellites and solar perturbations on the other hand, as well as by the Laplace resonance between Io, Europa and Ganymede. Current solutions for the ephemerides of the Galilean moons are mainly based on ground-based astrometric observations and space-based data from Voyager, Galileo, and Juno. For the numerical applications presented in this study (see Section 6), we choose as orbital theory for the Galilean satellites the numerical ephemerides JUP387 computed by R. Jacobson from JPL. It is available over the 1600 – 2400 time period. In Section 8.1, we quantify the changes in spin position obtained using the last version of NOE [Lainey et al., 2009] instead of JUP387.

Both JUP387 and the last version of NOE are represented by Chebyshev polynomials. However, a quasi-periodic decomposition of the orbital motion is particularly useful for computing the orientation/rotation of satellites. It is then possible to decompose the forcings into series and evaluate the rotational response term by term, retaining only the main terms of the solution. Using a Levenberg-Marquardt algorithm, we numerically fit the Laplace plane (see Section 2.2) on the 1600 – 2200 time period and the amplitudes, frequencies and phases of a periodic series

of at least 10 terms for the projected coordinates of the orbit normal onto the Laplace plane (n_x , n_y , see Section 2.3). The frequencies correspond to integer combinations of the fundamental arguments of the dynamical system. We use the numerical values of Lainey et al. [2006] as a priori values for the fit. A linear trend is also adjusted for each angle.

The fit residuals are usually less than 0.0002° .

2.2 The reference plane

As mentioned above, the rotation modeling community needs a fixed plane to serve as a reference plane for describing the orbital elements involved in the forcing torque and the resulting rotational response. The equator of Jupiter at epoch J2000 may be proposed as a fixed reference plane, as is usually the case to

	Io	Europa	Ganymede	Callisto
Laplace pole:				
α_{LP} (°)	268.0594 (268.05)	268.0850 (268.08)	268.2044 (268.20)	268.7322 (268.72)
δ_{LP} (°)	64.4968 (64.50)	64.5095 (64.51)	64.5683 (64.57)	64.8244 (64.83)
Transformation coefficients:				
$1/\cos \delta_{LP}$	2.3226	2.3236	2.3286	2.3508
$\tan \delta_{LP} / \cos \delta_{LP}$	4.8686	4.8737	4.8971	5.0011
$-1/2 \tan \delta_{LP}$	-1.0481	-1.0487	-1.0515	-1.0637
$\cos \delta_{LP}$	0.4306	0.4304	0.4294	0.4254
$-\sin \delta_{LP}$	-0.9026	-0.9027	-0.9031	-0.9050
$1/4 \sin 2\delta_{LP}$	0.1943	0.1942	0.1939	0.1925

Table 1: Numerical values for the orientation angles of the Laplace plane for the four Galilean satellites and transformation coefficients, using the JUP387 ephemerides. Values in parentheses are from Archinal et al. [2018]. The Jupiter pole coordinates are $\alpha_J = 268.0564^\circ$, $\delta_J = 64.4953^\circ$.

describe the orbital motion of the Galilean satellites. However, due to the influence of the Sun, Jupiter's equator is not the best reference plane to describe the rotational response of the satellites (see e.g. Noyelles [2009]). A relevant choice is the plane perpendicular to the center of the orbital cone for a regular motion, or for non-regular motion, that keeps the orbit inclination variations as small as possible. This reference plane is known as the Laplace plane. Since there are different ways to compute the Laplace plane (depending, for example, on the choice of the ephemerides, the time interval, or the quantity to minimize), different numerical estimations could be obtained. Our numerical values of the Laplace plane position for the four Galilean satellites are given in Table 1, using the JUP387 ephemerides. The farther the satellite is from the planet, the farther the Laplace plane is from Jupiter's equator.

2.3 Projection of the spin axis in the reference plane

Following the habits of the rotation modeling community (e.g. Bills [2005], Baland et al. [2012]), we introduce the components (n_x, n_y, n_z) of the unit vector along the orbit normal expressed in the coordinates of the Laplace reference frame:

$$n_x(t) = \sin i(t) \sin \Omega(t) \approx i(t) \sin \Omega(t), \quad (3a)$$

$$n_y(t) = -\sin i(t) \cos \Omega(t) \approx -i(t) \cos \Omega(t), \quad (3b)$$

$$n_z(t) = \cos i(t). \quad (3c)$$

The angle i corresponds to the angle i_{LO} in Fig. 1 ($i \approx \sqrt{n_x^2 + n_y^2}$) and the node longitude is $\Omega = \Omega_{ILLO}$. Similarly, the components (s_x, s_y, s_z) of the unit vector along the spin axis expressed in the coordinates of the Laplace reference frame are given by:

$$s_x(t) = \sin \theta(t) \sin \psi(t) \approx \theta(t) \sin \psi(t), \quad (4a)$$

$$s_y(t) = -\sin \theta(t) \cos \psi(t) \approx -\theta(t) \cos \psi(t), \quad (4b)$$

$$s_z(t) = \cos \theta(t). \quad (4c)$$

The inertial obliquity $\theta(t)$ is the angle between the spin axis and the Laplace pole i_{LS} ($\theta \approx \sqrt{s_x^2 + s_y^2}$). $\psi(t) = \Omega_{ILLS}$ is the node longitude of the equatorial plane along the Laplace plane, starting from the ICRF node.

As we will show in the next section, the components s_x and s_y are more convenient to transform to the right ascension/declination angles than the angles θ and ψ taken separately because s_x/s_y mainly present small periodic variations, while $\psi(t)$ is dominated by a large precession trend.

3 Transformation between the orientation angles α_S, δ_S and θ, ψ

In this section, we describe the precise transformation between the Euler and Earth equator orientation angles of the spin axis, which is independent of the rotation angles ϕ and W . We use as intermediate variables the components of the unit vector along the spin axis in the coordinates of the Laplace frame, $\hat{\mathbf{s}} = (s_x, s_y, s_z)$ which are defined in terms of θ and ψ , see Eqs. (4). The transformation described below is also valid for the orientation of the orbit normal, provided that the components $\hat{\mathbf{n}} = (n_x, n_y, n_z)$ of the unit vector along the orbit normal in the coordinates of the Laplace frame (Eqs. 3) are used as intermediate variables and subscript O is used instead of subscript S for the Earth equatorial angles.

3.1 Exact transformations

Using the classical spherical trigonometry or equivalently the equality between the rotation matrices $\mathbf{M}_{\theta\psi\phi}$ and $\mathbf{M}_{\alpha\delta W}$ of Eqs. (2), the exact transformations from the spin coordinates (s_x, s_y, s_z) with respect to the Laplace frame to the Earth equatorial angles (α_S, δ_S) are given by:

$$\sin \delta_S = s_y \cos \delta_{LP} + \sin \delta_{LP} s_z, \quad (5a)$$

$$\cos \delta_S \sin(\alpha_S - \alpha_{LP}) = s_x, \quad (5b)$$

$$\cos \delta_S \cos(\alpha_S - \alpha_{LP}) = \cos \delta_{LP} s_z - s_y \sin \delta_{LP}. \quad (5c)$$

The opposite transformations from the Earth equatorial angles to the spin coordinates in the Laplace frame are given by:

$$s_x = \cos \delta_S \sin(\alpha_S - \alpha_{LP}), \quad (6a)$$

$$s_y = \sin \delta_S \cos \delta_{LP} - \cos \delta_S \sin \delta_{LP} \cos(\alpha_S - \alpha_{LP}), \quad (6b)$$

$$s_z = \sin \delta_S \sin \delta_{LP} + \cos \delta_S \cos \delta_{LP} \cos(\alpha_S - \alpha_{LP}). \quad (6c)$$

We aim to express each angle/unit vector component as a sum of different parts, including periodic series. In order to maintain the representation in series for the periodic parts, approximate but accurate transformations are defined below.

3.2 Approximate transformations

With the exception of s_z , each angle and unit vector component is expressed as the sum of the Laplace pole value, a slow linear term with a rate noted tr , and a series noted Δ of periodic terms with small amplitudes:

$$s_x(t) = tr_x t + \Delta s_x(t), \quad (7a)$$

$$s_y(t) = tr_y t + \Delta s_y(t), \quad (7b)$$

$$s_z(t) = 1 + \Delta s_z(t), \quad (7c)$$

$$\alpha_S(t) = \alpha_{LP} + tr_\alpha t + \Delta \alpha_S(t), \quad (7d)$$

$$\delta_S(t) = \delta_{LP} + tr_\delta t + \Delta \delta_S(t), \quad (7e)$$

where t is the time. The Laplace pole values of (s_x, s_y, s_z) are by definition $(0, 0, 1)$. The values of α_{LP} and δ_{LP} depend on the chosen orbital model, see Section 2. The periodic terms Δs_x and Δs_y are the nutations in space of the spin axis (the dominant part of the nutational motion can be called precession). The periodic parts $\Delta \alpha_S(t)$ and $\Delta \delta_S(t)$ can also be called nutations. In the present context of approximate transformations, all these periodic variations are considered as first order terms. By construction, the spin models for s_x and s_y also contain secular terms. Since for the Galilean satellites they are much smaller than the largest periodic terms, these secular terms are considered to be of second order. Therefore, since the spin vector is unitary, $\Delta s_z \simeq -(\Delta s_x^2 + \Delta s_y^2)/2$ and is formally considered here as a second-order quantity. By construction, s_z should also include quadratic and Poisson terms. Very small quadratic and Poisson terms (product between a linear term and a periodic series) are neglected here in s_x/s_y and α_S/δ_S , because they are formally considered of order 3 or above and do not significantly improve accuracy in numerical applications.

To obtain approximate expressions for $\Delta\alpha_S$ and $\Delta\delta_S$, assuming that we have expressions for Δs_x and Δs_y , we express the exact trigonometric expressions of Eqs. (5) correct-up to the second-order in Δ quantities. Extracting $\Delta\alpha_S$ and $\Delta\delta_S$, we find:

$$\Delta\alpha_S = \frac{1}{\cos \delta_{LP}} \Delta s_x + \frac{\tan \delta_{LP}}{\cos \delta_{LP}} \Delta s_x \Delta s_y, \quad (8a)$$

$$\Delta\delta_S = \Delta s_y - \frac{1}{2} \tan \delta_{LP} \Delta s_x^2. \quad (8b)$$

The opposite transformation is given by:

$$\Delta s_x = \cos \delta_{LP} \Delta\alpha_S - \sin \delta_{LP} \Delta\alpha_S \Delta\delta_S, \quad (9a)$$

$$\Delta s_y = \Delta\delta_S + \frac{1}{4} \sin 2\delta_{LP} \Delta\alpha_S^2, \quad (9b)$$

$$\Delta s_z = -\frac{1}{2} (\cos^2 \delta_{LP} \Delta\alpha_S^2 + \Delta\delta_S^2). \quad (9c)$$

The transformation coefficients in Eqs. (8-9) depend on the Laplace plane orientation and slightly differ for each Galilean satellite. Numerical values of the first order coefficients for the four Galilean satellites are listed in Table 1. The second order transformation coefficients are usually between -1 and 5 . Similar expressions, but restricted to the first-order part of the transformation, apply to the small trends (tr quantities):

$$\cos \delta_{LP} tr_\alpha = tr_x, \quad (10a)$$

$$tr_\delta = tr_y. \quad (10b)$$

Since quadratic and Poisson terms are neglected here, their transformation relations are not given. Such transformations have been provided by Yseboodt et al. [2023] in the case of Mars.

The first order series in $\Delta\alpha_S$ and $\Delta\delta_S$ (Eqs. 8 without the second order terms) keep an analytical/trigonometrical form similar as that of s_x, s_y (that is to say, series with the same number of terms, at the same frequencies). The second-order terms result in additional periodic terms to the series, due to the recombination of sine and cosine factors. This recombination may introduce a small constant term in addition to the periodic series. Note that the distinction between first and second order is purely formal, and not based on the actual values of the amplitudes. Some of these second-order terms may be of larger amplitude than some of the first-order terms. For this reason, the second-order terms allow to improve the accuracy of the transformation (from 0.01° to less than 0.0001° in α , and from 0.006° to 0.0001° in δ), see Table 10 and Section 6.3.

3.3 Back to the obliquity and node longitude

The inertial obliquity and node longitude of the spin axis can be retrieved from the following exact relations:

$$\sin \theta = \sqrt{s_x^2 + s_y^2}, \quad (11a)$$

$$\psi = \arctan(-s_y, s_x). \quad (11b)$$

Similarly, the inclination and node longitude of the orbit normal are obtained as

$$\sin i = \sqrt{n_x^2 + n_y^2}, \quad (12a)$$

$$\Omega = \arctan(-n_y, n_x). \quad (12b)$$

The orbital obliquity (the angle between the orbit normal and the spin) is defined as:

$$\cos \varepsilon = \hat{\mathbf{n}} \cdot \hat{\mathbf{s}}. \quad (13)$$

We use the notation $\arctan(x, y)$ in the definitions for ψ and Ω to take into account the quadrant in which the point (x, y) lies. If we take into account the quadrant in which the projections of $\hat{\mathbf{s}}$ and $\hat{\mathbf{n}}$ onto the Laplace

plane lie when calculating ψ and Ω , then θ and i will be positive by default. This is convenient for satellites whose spin and orbit poles are on the same side with respect to the Laplace pole. For a satellite like the Moon, whose spin axis and orbit normal are located on opposite sides with respect to the Laplace pole, and thus their projections in opposite quadrants, it can be interesting from a modeling point of view (where ψ is generally assumed to be equal to or close to Ω) to change the sign of θ and add π to ψ . This is equivalent to redefining the descending node as the ascending node, but with a negative obliquity.

We can find valid approximations for the inertial obliquity θ and longitude ψ , either as a function of Δs_x and Δs_y , or as a function of $\Delta \alpha_S$ and $\Delta \delta_S$, using the relationship between the two sets of periodic variations, up to order 2:

$$\theta \approx \sqrt{\Delta s_x^2 + \Delta s_y^2} + \frac{(tr_x \Delta s_x + tr_y \Delta s_y)}{\sqrt{\Delta s_x^2 + \Delta s_y^2}} t, \quad (14a)$$

$$\approx \sqrt{\cos^2 \delta_{LP} \Delta \alpha_S^2 + \Delta \delta_S^2} - \frac{\Delta \alpha_S^2 \Delta \delta_S \sin 2\delta_{LP}}{4 \sqrt{\cos^2 \delta_{LP} \Delta \alpha_S^2 + \Delta \delta_S^2}} + \frac{(\cos^2 \delta_{LP} tr_\alpha \Delta \alpha_S + tr_\delta \Delta \delta_S)}{\sqrt{\cos^2 \delta_{LP} \Delta \alpha_S^2 + \Delta \delta_S^2}} t, \quad (14b)$$

$$\psi \approx \arctan(-\Delta s_y, \Delta s_x) + \frac{(tr_y \Delta s_x - tr_x \Delta s_y)}{\Delta s_x^2 + \Delta s_y^2} t \quad (14c)$$

$$\approx \arctan(-\Delta \delta_S, \cos \delta_{LP} \Delta \alpha_S) + \frac{1}{2} \Delta \alpha_S \sin \delta_{LP} \left(\frac{\Delta \alpha_S^2 \cos^2 \delta_{LP} + 2\Delta \delta_S^2}{\Delta \delta_S^2 + \Delta \alpha_S^2 \cos^2 \delta_{LP}} \right) + \frac{(tr_\delta \Delta \alpha_S - tr_\alpha \Delta \delta_S) \cos \delta_{LP}}{\Delta \delta_S^2 + \Delta \alpha_S^2 \cos^2 \delta_{LP}} t. \quad (14d)$$

Due to the linear terms in s_x and s_y (or in α_S and δ_S), these relations contain some terms proportional to the linear rates $tr_{x/y/\alpha/\delta}$ that we here keep since they ensure a higher degree of precision (e.g. error $\leq 0.0001^\circ$ for Europa's inertial obliquity compared to the solution obtained with Eq. (11a), instead of 0.002° without Poisson terms). For Io, those terms contribute up to 6° in ψ after 100 years, see section 6.2.

As mentioned in the introduction to this section, the transformations of Section 3.2 also apply to $\hat{\mathbf{n}} = (n_x, n_y, n_z)$ and (α_O, δ_O) . Therefore similar relationships as Eqs. (14) exist for the inclination i and node longitude Ω , with Δn_x and Δn_y instead of Δs_x and Δs_y and $\Delta \alpha_O$ and $\Delta \delta_O$ instead of $\Delta \alpha_S$ and $\Delta \delta_S$. For the same reason, this also allows us to find a workable expression for the orbital obliquity ε :

$$\varepsilon \approx \sqrt{(\Delta s_x - \Delta n_x)^2 + (\Delta s_y - \Delta n_x)^2}, \quad (15a)$$

$$\approx \sqrt{\cos^2 \delta_{LP}^2 (\Delta \alpha_S - \Delta \alpha_O)^2 + (\Delta \delta_S - \Delta \delta_O)^2} - \frac{(\Delta \alpha_O - \Delta \alpha_S)^2 (\Delta \delta_O + \Delta \delta_S) \sin 2\delta_{LP}}{4 \sqrt{\cos^2 \delta_{LP}^2 (\Delta \alpha_S - \Delta \alpha_O)^2 + (\Delta \delta_S - \Delta \delta_O)^2}}. \quad (15b)$$

The orbital obliquity is unaffected by the long-term trends. The first-order part of Eq. (15b) can be used to propagate errors from the IAU orientation angles to the orbital obliquity.

3.4 Offset with respect to the Cassini plane

If the satellite's orbit and spin precess regularly at a constant rate and if the satellite is unaffected by tidal dissipation, then the Laplace pole $\hat{\mathbf{l}}$, the orbit normal $\hat{\mathbf{n}}$ and the spin axis $\hat{\mathbf{s}}$ belong to the same plane, known as the Cassini plane. The Cassini plane is defined as the plane containing both the Laplace pole and the orbit normal. Due to irregular orbital precession and/or coupling with polar motion and/or tidal dissipation, the spin axis is in fact almost never in the Cassini plane. The offset ζ of the spin axis with respect to the Cassini plane can be written as, see Yseboodt and Margot [2006], Baland et al. [2017]:

$$\sin \zeta = \frac{\hat{\mathbf{l}} \times \hat{\mathbf{n}}}{\|\hat{\mathbf{l}} \times \hat{\mathbf{n}}\|} \cdot \hat{\mathbf{s}}. \quad (16)$$

With this sign convention, the offset is defined as a prograde angle. In the case of a dissipative body with a regular retrograde orbital precession, a positive offset indicates a spin axis lagging "behind" the Cassini plane.

Using the expressions of the $\hat{\mathbf{n}}$ and $\hat{\mathbf{s}}$ vectors and since $\hat{\mathbf{I}} = (0, 0, 1)$ in the Laplace Frame, Eq. (16) can be reduced to

$$\zeta \simeq \frac{\Delta n_x \Delta s_y - \Delta n_y \Delta s_x}{\sqrt{\Delta n_x^2 + \Delta n_y^2}} + \frac{(\Delta n_x (\Delta n_x - \Delta s_x) + \Delta n_y (\Delta n_y - \Delta s_y))}{(\Delta n_x^2 + \Delta n_y^2)^{3/2}} (tr_y \Delta n_x - tr_x \Delta n_y) t, \quad (17a)$$

$$\begin{aligned} &\simeq \frac{(\Delta \alpha_O \Delta \delta_S - \Delta \alpha_S \Delta \delta_O) \cos \delta_{LP}}{\sqrt{\Delta \delta_O^2 + \Delta \alpha_O^2 \cos^2 \delta_{LP}}} \\ &+ t \frac{(\Delta \alpha_O tr_\delta - \Delta \delta_O tr_\alpha) (\Delta \delta_O (\Delta \delta_O - \Delta \delta_S) + \Delta \alpha_O (\Delta \alpha_O - \Delta \alpha_S) \cos^2 \delta_{LP}) \cos \delta_{LP}}{(\Delta \delta_O^2 + \Delta \alpha_O^2 \cos^2 \delta_{LP})^{3/2}} \\ &+ \frac{\sin \delta_{LP} (\Delta \alpha_S - \Delta \alpha_O) (2 \Delta \delta_O^3 \Delta \delta_S + \Delta \alpha_O^3 \Delta \alpha_S \cos^4 \delta_{LP})}{2 (\Delta \delta_O^2 + \Delta \alpha_O^2 \cos^2 \delta_{LP})^{3/2}} \\ &- \frac{\sin \delta_{LP} \Delta \alpha_O \Delta \delta_O \cos^2 \delta_{LP} (\Delta \alpha_O^2 \Delta \delta_S + 2 \Delta \alpha_O \Delta \alpha_S (\Delta \delta_O - \Delta \delta_S) - \Delta \alpha_S^2 \Delta \delta_O)}{2 (\Delta \delta_O^2 + \Delta \alpha_O^2 \cos^2 \delta_{LP})^{3/2}}. \end{aligned} \quad (17b)$$

The first term of Eq. (17a) corresponds to Eq. (9) of Baland et al. [2011].

4 Transformation between the rotation angles ϕ and W

The rotation angles ϕ and W describe the location of the intersection between the prime meridian and the equator of the satellite, measured from the node of the equator over the Laplace plane and over the Earth mean equator of J2000, respectively. In this section, we now use the notation ϕ_{Euler} for the Euler rotation angle, to distinguish it from other rotation angles also noted with the letter ϕ and measured from a different origin, see Section 4.3.

We assume for the rotation angles a generic form with an initial value at epoch, a linear term, and a series of small periodic variations ($\Delta \phi_{Euler}$ and ΔW are related to the librations in longitude, see Section 4.3):

$$\phi_{Euler}(t) = \phi_0 + \dot{\phi} t + \Delta \phi_{Euler}(t), \quad (18a)$$

$$W(t) = W_0 + \dot{W} t + \Delta W(t). \quad (18b)$$

The difference between the rotation angles W and ϕ_{Euler} is the angle β corresponding to the angle Ω_{ISLS} in Fig. 1:

$$W = \phi_{Euler} + \beta. \quad (19)$$

It is measured along the equator of the satellite from the node with the ICRF to the node with the Laplace plane.

4.1 Exact transformation

The β angle is not constant with time due to the precessional motion of the equator but does not intervene in the transformations between orientation angles of Section 3. Its cosine and sine can be written as a function of the Euler orientation angles ψ and θ and the declinations of the spin axis (δ_S) and Laplace pole (δ_{LP}) as follows:

$$\cos \beta = \frac{\cos \delta_{LP} \cos \psi \cos \theta + \sin \delta_{LP} \sin \theta}{\cos \delta_S}, \quad (20a)$$

$$\sin \beta = \frac{\cos \delta_{LP} \sin \psi}{\cos \delta_S}, \quad (20b)$$

which leads to (still using the notation $\arctan(x, y)$ for a point of coordinates (x, y))

$$\beta(t) = \arctan(\cos \beta, \sin \beta) = \arctan(\cos \psi \cos \theta + \tan \delta_{LP} \sin \theta, \sin \psi), \quad (21)$$

where $\sin \theta = \sqrt{s_x^2 + s_y^2}$ and $\cos \theta = \sqrt{1 - s_x^2 - s_y^2}$.

4.2 Approximate transformation

Using the approximate expressions for s_x and s_y of Eqs. (7a-7b) and the transformation relationship between the different sets of orientation angles, we now find approximations for β , either as a function of tr_x , Δs_x and Δs_y , or as a function of tr_α , $\Delta \alpha_S$ and $\Delta \delta_S$ (we neglect quadratic and Poisson terms):

$$\beta(t) \approx \psi(t) - \tan \delta_{LP} tr_x t - \tan \delta_{LP} \Delta s_x - \left(\tan^2 \delta_{LP} + \frac{1}{2} \right) \Delta s_x \Delta s_y, \quad (22a)$$

$$\approx \psi(t) - \sin \delta_{LP} tr_\alpha t - \sin \delta_{LP} \Delta \alpha_S - \frac{1}{2} \cos \delta_{LP} \Delta \alpha_S \Delta \delta_S. \quad (22b)$$

From these expressions, we can see that, although the two angles do not belong to the same plane, β and ψ have fairly close values at all times (maximum difference of around 0.7° for Ganymede). They both exhibit a precession (linear trend) which causes them to deviate relatively rapidly from their epoch values. In the following, we define the difference between β and ψ as the angle μ , that includes the difference between the trends and periodic variations of the two angles:

$$\mu = \beta - \psi \approx tr_\mu t + \Delta \mu(t), \quad (23a)$$

$$tr_\mu \approx -\tan \delta_{LP} tr_x \quad (23b)$$

$$\approx -\sin \delta_{LP} tr_\alpha, \quad (23c)$$

$$\Delta \mu(t) \approx -\tan \delta_{LP} \Delta s_x - \left(\tan^2 \delta_{LP} + \frac{1}{2} \right) \Delta s_x \Delta s_y, \quad (23d)$$

$$\approx -\sin \delta_{LP} \Delta \alpha_S - \frac{1}{2} \cos \delta_{LP} \Delta \alpha_S \Delta \delta_S. \quad (23e)$$

4.3 The different definitions of ϕ , in relation to the different definitions of the libration angle γ

Librations in longitude are defined as the periodic variations of the satellite's rotation around its spin axis. We have just defined two different rotation angles (ϕ_{Euler} and W), whose periodic variations $\Delta \phi_{Euler}$ and ΔW are different from each other, since β and ψ varies periodically with time. Clearly, if the definition of the rotation angle is not unique, neither is that of libration. The rotation modeling community still uses other definitions, based on dynamic considerations.

To resolve for the rotation variations with respect to synchronicity with the orbital motion, the gravitational torque in libration models depends on the difference between a rotation angle and the orbital true longitude (see Section 5.2), with both angles measured from the same origin. The choice of a fixed/inertial origin is necessary to correctly describe the torque and find a realistic libration motion. The most elementary libration model considers that the satellite evolves on a non-precessing eccentric Keplerian orbit (which can therefore be assimilated, for modeling purposes only, to both a reference plane instead of the Laplace plane and to the satellite's equator) and that it undergoes diurnal libration such that the satellite's long axis points towards the central body at pericenter (e.g. Van Hoolst et al. 2008). In this context, it makes sense to measure the angle of rotation on the plane of the orbit, starting from the pericenter. We note that rotation angle $\phi_{pericenter}$. It is also customary to refer the satellite's orbit not to its Laplace plane, but to Jupiter's equatorial plane, since in this modeling context, the Laplace plane is not of paramount importance. The geometric relationship between ϕ_{Euler} and $\phi_{pericenter}$, at first order in small angles i , θ and ε is

$$\Omega_{IQIL} + \psi + \phi_{Euler} = \Omega_{JupEq} + \omega_{JupEq} + \pi + \phi_{pericenter}, \quad (24)$$

where both the left and right hand sides are the broken angle starting at the point IQ in Fig. 1 and ending at the meridian plane, whereas the ϕ angles start at different points. Ω_{JupEq} is the node longitude of the orbit starting from the intersection between the ICRF equator and Jupiter Equator at J2000 and ω_{JupEq} is the argument of the satellite pericenter with respect to Jupiter Equator. $\omega_{JupEq} + \pi$ is the argument of the pericenter of the planet around the satellite. The Ω_{IQIL} angle is constant, since it is defined by three inertial planes. For a Keplerian non-precessing orbit, ψ , Ω_{JupEq} and ω_{JupEq} can be considered constant as well, so that $\Delta \phi_{Euler} = \Delta \phi_{pericenter}$ and is essentially diurnal.

However, the orbit pericenter is not a fixed point in space. The angle ω_{JupEq} is linearly and periodically perturbed. The modeler interested in a detailed rotation theory where librations also occur at periods other than the diurnal period needs to refer the rotation angle to another point. The node of the orbital plane is not fixed in space (Ω_{JupEq} is also linearly and periodically perturbed), and is not a more convincing starting point. The point IQ is a suitable choice, so that the left-hand side in Eq. (24) can be defined as the rotational angle $\phi_{Inertial}$:

$$\phi_{Inertial} = \Omega_{IQIL} + \psi + \phi_{Euler}. \quad (25)$$

The points IL and QL could also be suitable, since the triangle defined by the points IQ, QL, and IL is fixed. Depending on the actual starting point (IQ, IL or QL), $\phi_{Inertial}$ is defined to within one constant, just as Ω_{JupEq} .

In the most elementary libration model (e.g. Van Hoolst et al. 2008), the rotation angle is expressed as the sum of the mean anomaly and the small libration angle:

$$\phi_{pericenter} = M(t) + \gamma = M_0 + n_M t + \gamma \quad [\text{for a Keplerian orbit}], \quad (26)$$

where $M(t)$ only varies linearly at the rate n_M and γ is proportional to the eccentricity e and $\sin M$, so that the satellite's major axis always points approximately towards the orbit's empty focus, and the angle of rotation is the sum of an epoch value, of a linear trend representative of synchronous rotation, and of a single periodic term. For more advanced modeling, a similar formulation should be used, where $M(t)$ is replaced by the mean mean longitude L or by the mean longitude \mathcal{L} (following here the notations in Lainey et al. [2006]), both measured along Jupiter's equator:

$$\phi_{Inertial} = L(t) + \pi + \gamma_u, \quad (27a)$$

$$\phi_{Inertial} = \mathcal{L}(t) + \pi + \gamma_f, \quad (27b)$$

with

$$L(t) = L_0 + n_L t, \quad (28a)$$

$$\mathcal{L}(t) = \Omega_{JupEq}(t) + \omega_{JupEq}(t) + M(t) = L(t) + \Delta\mathcal{L}, \quad (28b)$$

$$\Delta\mathcal{L} = \Delta\Omega_{JupEq} + \Delta\omega_{JupEq} + \Delta M. \quad (28c)$$

The origin of L and \mathcal{L} is the intersection IQ between the ICRF equator and Jupiter Equator at J2000. By definition, L varies only linearly, whereas $\Delta\mathcal{L}$ also includes the periodic variations in Ω_{JupEq} , ω_{JupEq} , and M . The mean motion n_L of the mean longitude is the sum of the mean rates of the node longitude, of the pericenter argument, and of the mean anomaly, and differs from the mean motion of the mean anomaly n_M :

$$n_L = \dot{\Omega}_{JupEq} + \dot{\omega}_{JupEq} + n_M. \quad (29)$$

If the orbit is close to singular (this is the case for the Galilean satellites), these trends may be difficult to fit separately.

Eqs. (27) define two different small libration angles (γ_u and γ_f). γ_u defines the rotation increment with respect to a uniform rotation at rate n_L , whereas γ_f defines the increment with respect to a rotation that follows the forcing and is therefore in synchronicity with the mean longitude. γ_f has an obvious dynamic meaning, but γ_u might be more practical for describing observations. The connection between these two libration angles lies in the periodic variations of the mean longitude:

$$\gamma_f = \gamma_u - \Delta\mathcal{L}. \quad (30)$$

For a strictly Keplerian orbit, the two libration angles are equivalent: $\gamma_f = \gamma_u$.

Observations of a satellite's rotation can also be expressed not in terms of ϕ_{Euler} or $\phi_{Inertial}$, but in terms of the Earth equatorial angle W . Making use of Eqs. (19), (23a), (25) and (27), we have that

$$W = \mu + \pi - \Omega_{IQIL} + L + \gamma_u, \quad (31a)$$

$$= \mu + \pi - \Omega_{IQIL} + \mathcal{L} + \gamma_f. \quad (31b)$$

The rate of W is

$$\dot{W} = n_L + tr_\mu \approx n_L - \tan \delta_{LP} tr_x \quad (32)$$

and the periodic part of W is given by:

$$\Delta W = \Delta\mu + \gamma_u, \quad (33a)$$

$$= \Delta\mu + \Delta\mathcal{L} + \gamma_f, \quad (33b)$$

with $\Delta\mu$ the periodic part of $\mu = \beta - \psi$, see Eq. (23a).

With the latter expressions, the meaning of μ becomes clearer. If β represents the transformation between W and ϕ_{Euler} , then μ represents, to within one constant, the transformation between W and $L + \gamma_u$ (or equivalently between W and $\mathcal{L} + \gamma_f$), or more simply, between W and $\phi_{inertial}$:

$$W = \phi_{Inertial} + \mu - \Omega_{IQIL}. \quad (34)$$

4.4 Back to ϕ_{Euler}

We assume here that measuring the orientation and rotation of a satellite involves either the set of quantities $(\Delta s_x, \Delta s_y, \gamma_{f/u})$, or $(\Delta\alpha_S, \Delta\delta_S, \Delta W)$, depending on whether the observer is using a representation close to Euler angles or terrestrial equatorial coordinates. The angle ϕ_{Euler} , unlike $\phi_{Inertial}$ (and therefore $\gamma_{u/f}$), would be impractical as an observable, as it cannot be observed without a concomitant determination of ψ . However, ϕ_{Euler} is required to express the rotation matrix (Eq. 2a) in terms of Euler angles.

From a measurement of $\gamma_{u/f}$ and the expression of $\phi_{Inertial}$, see Eq. (27), we can simply obtain the expression of ϕ_{Euler} from Eq. (25) as follows

$$\phi_{Euler} = L(t) + \pi + \gamma_u - \Omega_{IQIL} - \psi, \quad (35a)$$

$$\phi_{Euler} = \mathcal{L}(t) + \pi + \gamma_f - \Omega_{IQIL} - \psi, \quad (35b)$$

where ψ is obtained from measurements of Δs_x and Δs_y and Eq. (14c).

From a measurement of ΔW and Eq. (33), it is possible to obtain the expression for $\gamma_{u/f}$ if the expression for $\Delta\mu$ is first derived from the measured $(\Delta\alpha_S, \Delta\delta_S)$ with Eq. (23e):

$$\gamma_u = \Delta W - \Delta\mu, \quad (36a)$$

$$\gamma_f = \Delta W - \Delta\mu - \Delta\mathcal{L}. \quad (36b)$$

ϕ_{Euler} is then obtained as described in the previous paragraph. In a more direct way, without going through $\gamma_{u/f}$ but calculating β with Eq. (22b) from the measured $(\Delta\alpha_S, \Delta\delta_S)$, we can use

$$\phi_{Euler} = W - \beta \quad (37)$$

to obtain ϕ_{Euler} from the measured W .

The rate of ϕ_{Euler} is

$$\dot{\phi}_{Euler} = n_L - \dot{\psi}. \quad (38)$$

5 Dynamical models

The Galilean satellites are assumed to be locked in the Cassini state, with their rotation variations described as a combination of variations in the rotation angle (librations, as defined in Section 4.3), variations in the orientation of the spin axis in space (nutations, as defined in Section 3.2), and variations in the orientation of the spin axis relative to the Body Frame (polar motion). These rotation variations are caused by the external gravitational torque exerted by Jupiter on the flattened shape of the satellites. In the case of Titan, in addition to the external torque exerted by Saturn, angular momentum exchanges between the atmosphere and lakes and the solid surface also contribute to the rotation variations (the resulting variations in rotation around the spin axis are then called length-of-day variations). In this section, we identify relevant dynamical models to create Euler angle solutions to be transformed into equatorial coordinates in Section 6.3. Since we provide a

transformation method for series of rotation variations, we are only interested here in rotation models whose solution is expressed in series.

Series for rotational variations can be modeled within the angular momentum (AM) framework, by solving equations that relate the rate of change of the rotation AM to the external torques applied. The AM equations can be solved numerically, before a frequency analysis is applied to the solution (e.g. Rambaux et al. [2011]). Fitted series for the rotational variations can also be obtained within an Hamiltonian framework (e.g. Noyelles [2009]). Another way of approaching the problem is to solve the AM equations analytically, using a semi-analytical orbital theory to express the forcing, so that the solution is directly expressed in series (e.g. Bills 2005, Baland et al. 2012, Yseboodt and Van Hoolst 2014). The latter approach requires a number of working assumptions, particularly with regard to the quantities and terms that can be neglected or not. Such a series obtained from an analytical solution will generally contain fewer terms than a series fitted from a numerical solution. Nevertheless, by extending an analytical solution to a sufficient order, it should be possible to recover a sufficient number of terms and tend towards the numerical solution. For example, Coyette et al. [2025] recently extended an analytical AM theory to the second order in small quantities and recovered rotational variation terms that had previously only been identified from a frequency analysis. Here we will provide simplified dynamical models (analytical AM models developed to the first order in small quantities) identified in the literature. Providing a very detailed theory of the rotation of Galilean satellites is outside the scope of the present study and is not necessary to assess the accuracy of the transformations defined in Sections 3 and 4.

Note that the transformation between (s_x, s_y) and (α_S, δ_S) requires only knowledge of the orientation of the Laplace plane, and is therefore independent of the details of the internal structure. On the other hand, the transformation between W and ϕ_{Euler} (or $L + \gamma_u = \mathcal{L} + \gamma_f$), namely $\beta(\mu)$, requires knowledge of the orientation of both the Laplace plane and the spin axis, and therefore depends on the internal structure. In the absence of spin orientation measurements, this transformation is dependent on the theoretical model chosen to simulate the spin axis precession. Finally, note that neither the transformation between (s_x, s_y) and (α_S, δ_S) nor that between W and ϕ_{Euler} depends on the librations $\gamma_{u/f}$. We will illustrate the transformation and provide an example of numerical series for the spin orientation model $(\alpha_S, \delta_S$ and $W)$ in the solid case, see Section 6. The equations for the libration dynamical model are provided here for completeness and illustration purposes. Our goal in this study is not to solve them, but to link the different libration angles definitions that exist in the literature (see Section 4.3) and to show corresponding appropriate dynamical equations.

5.1 Spin orientation model

For a fully rigid triaxial satellite, we will use the model of Baland et al. [2011], where the variations of $\hat{\mathbf{s}}$ are described in an inertial reference frame linked to the Laplace plane:

$$nC \frac{d\hat{\mathbf{s}}}{dt} = n\kappa(\hat{\mathbf{s}} \wedge \hat{\mathbf{n}}), \quad (39a)$$

$$\kappa = \frac{3}{2}MR^2(-C_{20} + 2C_{22})n = \frac{3}{2}(C - A)n. \quad (39b)$$

This model is developed to first order in inclination and obliquity and assumes that spin precession in space is decoupled from librations and polar motion. As stated in Section 2.3, $\hat{\mathbf{s}}$ is the unit vector along the spin axis and $\hat{\mathbf{n}}$ is the unit vector along the orbit normal. n is the mean motion while the mass and the radius of the satellite are M and R . C_{20} and C_{22} are the second-degree gravity field coefficients of the satellite, which can be expressed in terms of $A < B < C$, the principal moments of inertia. If the satellite's orbit is precessing uniformly at the rate $\dot{\Omega}$ and with inclination i , the orbital obliquity is obtained as

$$\varepsilon = -\frac{i\dot{\Omega}}{\dot{\Omega} + \kappa/C}, \quad (40)$$

an expression that is consistent with the majority of the literature (e.g. Noyelles 2010, Henrard and Schwanen 2004, Boué 2020, Coyette et al. 2025). Bills [2005] and Bills and Nimmo [2011] obtain different solutions,

due to their incorrect definitions of the coupling constant κ . The exact expression of Eq. (39) has been demonstrated in Appendix A of Baland et al. [2012].

Interestingly, Eq. (39) can be transformed into a couple of differential equations for the right ascension α_S and declination δ_S of the rotation axis with respect to the ICRF. With the ICRF coordinates (α_S, δ_S) and (α_O, δ_O) , the spin and orbit unit vectors are expressed in the coordinates of the ICRF as

$$\hat{\mathbf{s}} = (\cos \alpha_S \cos \delta_S, \cos \delta_S \sin \alpha_S, \sin \delta_S), \quad (41a)$$

$$\hat{\mathbf{n}} = (\cos \alpha_O \cos \delta_O, \cos \delta_O \sin \alpha_O, \sin \delta_O), \quad (41b)$$

so that

$$\frac{d\alpha_S}{dt} = \frac{\kappa}{C} (\cos \delta_O \tan \delta_S \cos(\alpha_O - \alpha_S) - \sin \delta_O), \quad (42a)$$

$$\frac{d\delta_S}{dt} = \frac{\kappa}{C} \cos \delta_O \sin(\alpha_O - \alpha_S). \quad (42b)$$

In the limit of small orbital obliquity and neglecting tidal dissipation, Eqs. (42) correct Eqs. (E4-E5) of Bills and Scott [2022] as obtained from their Eq. 4.8 (with $\hat{\mathbf{s}} \cdot \hat{\mathbf{n}} \sim 1$ and $p_3 = 0$). Eqs. (42) can be integrated numerically to provide a benchmark for assessing the accuracy of the transformation presented in section 3.

For the case where the satellites harbor an internal global liquid layer, as will be considered in Section 8.2, we will use the solution presented in Appendix 5 of Baland et al. [2019], which extends the model of Baland et al. [2011, 2012] by including the hydrodynamic pressure (Poincare flow) at the interfaces between the ocean and the solid layers. That model assumes that the solid layers behave rigidly.

5.2 Libration model

The dynamical equation for solving librations can be obtained as the third component of the AM equation expressed in the rotating BF :

$$\frac{\partial \mathbf{L}}{\partial t} + \boldsymbol{\Omega} \wedge \mathbf{L} = \mathbf{N}, \quad (43)$$

where $\boldsymbol{\Omega} = (\omega_x, \omega_y, \omega_z)$ is the rotation vector, $\mathbf{N} = (N_x, N_y, N_z)$ is the total torque exerted on the satellite, and \mathbf{L} is the angular momentum. For a fully rigid triaxial satellite, $L_z = C \omega_z$ with $\omega_z \simeq \dot{\psi} + \dot{\phi}_{Euler} = \dot{\phi}_{Inertial}$ at first order in θ and the libration equation reads, see also Eqs. (5.48) of Murray and Dermott [2000]:

$$C \dot{\omega}_z - (A - B) \omega_x \omega_y = N_z. \quad (44)$$

In a simple first order theory, the product of the polar motion components ω_x and ω_y can be neglected and N_z approximated at first order in small quantities, so that

$$C \ddot{\phi}_{Inertial} = -\frac{3}{2}(B - A) \frac{GM_J}{d^3} \sin 2(\phi_{Inertial} - l_{JupEq}), \quad (45)$$

with d the distance between the satellite and the parent planet and $l_{JupEq} = \Omega_{JupEq} + \omega_{JupEq} + f$ the true longitude of the satellite. M_J is the mass of Jupiter and G is the universal gravitational constant. The difference $(\phi_{Inertial} - l_{JupEq})$ is the angle from the direction of the satellite long axis (corresponding to the principal moment of inertia A) to the direction to the central planet. Since the sine argument is a small quantity, it can replace the sine factor.

For a Keplerian orbit, with $GM_J = n^2 a^3$, with n and a the mean motion and semi-major axis, respectively, Eq. (45) simplifies to

$$C \ddot{\phi}_{pericenter} = -\frac{3}{2}n^2(B - A) \left(\frac{a}{d}\right)^3 \sin 2(\phi_{pericenter} - f) \quad [\text{For a Keplerian orbit}], \quad (46)$$

with f the true anomaly, see e.g. Eq. (1) of Van Hoolst et al. [2008]. The right-hand side of the equation can first be expressed as series in eccentricity e before solving the dynamical equation. The solution consists in a main diurnal librations and smaller terms at harmonics of the orbital period.

Orbital perturbations lead to changes in the gravitational torque of Jupiter on the satellite compared to the torque in the Keplerian case. Based on the chosen orbital theory, the factor of $\sin 2(\phi_{Inertial} - l_{JupEq})/d^3$ can first be expressed as series before solving the dynamical equation. Depending on the chosen definition for the libration angle (with respect to the forcing γ_f or with respect to the uniform rotation γ_u), Eq. (45) can take two different forms:

$$C(\ddot{\gamma}_f + \ddot{L}) = -\frac{3}{2}(B-A) \frac{GM_J}{d^3} \sin(2\gamma_f + 2M - 2f), \quad (47a)$$

$$C\ddot{\gamma}_u = -\frac{3}{2}(B-A) \frac{GM_J}{d^3} \sin(2\gamma_u + 2L - 2l_{JupEq}). \quad (47b)$$

In addition to the diurnal (+ harmonics) libration, other libration terms arise due to the orbital perturbations.

6 Spin orientation series and transformation accuracy

In this section, we assess the accuracy of the transformations defined in Sections 3 and 4 for the orientation and rotation angles of the Galilean satellites. As we pointed out at the start of Section 5, the coefficients for the transformation of the orientation angles depend only on the orientation of the Laplace plane (through α_{LP} and δ_{LP}), whereas the β and μ angles for the transformation of the rotation angles also depend on the orientation of the spin axis (α_S, δ_S), the latter being dependent on the internal structure of the satellites. We first build series for the spin axis coordinates (s_x, s_y) for satellites assumed to be entirely solid and rigid. This is an update of the corresponding series of Baland et al. [2012] using more recent orbital ephemerides. Then we build the corresponding series in orientation and rotation angles, both for Euler ($\theta, \psi, \varepsilon, \zeta$) or Earth equatorial (α_S, δ_S) angles. The effect of an internal ocean on the orientation angles, and consequently on the rotation angles' transformation μ , is discussed in Section 8.2.

6.1 Spin orientation series for solid Galilean satellites, in (s_x, s_y)

Following the decomposition described in Section 2.1, the orbit normal coordinates (n_x, n_y) are written as the sum of a linear term (with the tr_x and tr_y rates, second order terms by construction) and of a trigonometric series (noted Δ , and of first order by construction):

$$n_x(t) \approx tr_x t + \Delta n_x = tr_x t + \sum_j i_j \sin(f_j t + \varphi_j), \quad (48a)$$

$$n_y(t) \approx tr_y t + \Delta n_y = tr_y t - \sum_j i_j \cos(f_j t + \varphi_j), \quad (48b)$$

where i_j are the inclination amplitudes associated with the orbital node precession frequencies f_j and the phases φ_j , and t is the time. For each inclination amplitude i_j in the forcing, there is a corresponding inertial obliquity amplitude

$$\theta_j = i_j + \varepsilon_j \quad (49)$$

in the satellite response, calculated using Eq. (40) and the value of the parameters listed in Table 2, so that the spin axis coordinates (s_x, s_y) are written as follows (see also Eq. 7):

$$s_x(t) = tr_x t + \Delta s_x = tr_x t + \sum_j \theta_j \sin(f_j t + \varphi_j), \quad (50a)$$

$$s_y(t) = tr_y t + \Delta s_y = tr_y t - \sum_j \theta_j \cos(f_j t + \varphi_j). \quad (50b)$$

The linear terms, due to their very long period, are left unchanged by the external gravitational torque, and are therefore identical for n_x and s_x and for n_y and s_y .

The values of the trends tr_x and tr_y are given in Table 3, whereas the values of the amplitudes i_j , ε_j and θ_j , frequencies f_j and phases φ_j are given in Table 4, for the four Galilean satellites, considering a

	M (10^{23} kg)	R (km)	n_L (rad/d)	A/MR^2	C/MR^2	$2\pi/\omega_f$ (y)	surface shift (km/ $^\circ$)
Io	0.892965	1821.49	3.551552313	0.376425	0.379538	0.3937	31.791
Europa	0.479857	1560.8	1.769322718	0.354277	0.354992	3.2189	27.241
Ganymede	1.481478	2631.2	0.878207920	0.311381	0.311585	19.9407	45.923
Callisto	1.075661	2410.3	0.376486233	0.354869	0.354922	203.605	42.068

Table 2: Values for the mass (M), radius (R), mean motion (n_L), normalized principal moments of inertia A/MR^2 and C/MR^2 , and free precession period ($2\pi/\omega_f$) of the four Galilean satellites. The moments of inertia A and C are derived from the observed J_2 and C_{22} gravitational coefficients and from the mean moment of inertia I (see Anderson et al. [2001] for Io, Gomez Casajus et al. [2021] for Europa and Schubert et al. [2004] for Ganymede and Callisto). The n_L values are computed from JUP387 and differ from those in Lainey et al. [2006] by less than $3 \cdot 10^{-8}$ rad/d. The last column evaluates the amplitude at the satellite surface of an arbitrary angular displacement of 1° .

	tr_x ($^\circ$ /y)	$tr_y = tr_\delta$ ($^\circ$ /y)	tr_α ($^\circ$ /y)	tr_μ ($^\circ$ /y)	\dot{W} ($^\circ$ /d)	δ_{S0} ($^\circ$)
Io	$-2.8 \cdot 10^{-5}$	$2.4 \cdot 10^{-5}$	$-6.5 \cdot 10^{-5}$	$5.9 \cdot 10^{-5}$	203.488958424	$-1.4 \cdot 10^{-5}$
Europa	$-2.8 \cdot 10^{-5}$	$2.4 \cdot 10^{-5}$	$-6.4 \cdot 10^{-5}$	$5.9 \cdot 10^{-5}$	101.374724491	$-2.49 \cdot 10^{-3}$
Ganymede	$-2.8 \cdot 10^{-5}$	$2.5 \cdot 10^{-5}$	$-6.5 \cdot 10^{-5}$	$5.9 \cdot 10^{-5}$	50.317607524	$-4.7 \cdot 10^{-4}$
Callisto	$-2.8 \cdot 10^{-5}$	$2.7 \cdot 10^{-5}$	$-6.5 \cdot 10^{-5}$	$5.9 \cdot 10^{-5}$	21.571072373	$-1.47 \cdot 10^{-3}$

Table 3: Trends in the various quantities considered. The tr_x and tr_y trends, obtained from the JUP387 orbital theory, apply to both the orbit normal and spin axis coordinates n/s_x and n/s_y , respectively. The tr_α , tr_δ and tr_μ trends are obtained after the transformation described in Eqs. (10) and (23b). The rotation rate in W is obtained from Eq. (32). The last column shows the small increment in δ_S due to the power reduction of a squared sine term in the second-order part of Eq. (8b).

solid interior model and the JUP387 orbital theory. The corresponding temporal evolution of the spin axis coordinates (s_x, s_y) in the Laplace plane is shown in Fig. 2.

In Table 4, we have considered a truncation threshold of the order of 0.0001° on the i_j , corresponding to the order of magnitude of the residuals in the orbit orientation angles between JUP387 and its frequency decomposition. We thus obtain 6, 10, 9, and 8 terms for Io, Europa, Ganymede, and Callisto, respectively. The arguments (frequencies and phases) of the series result from the orbital dynamics and are combinations of the fundamental arguments associated with the Jovian system (see last columns). However, arguments identified as being the same combination may have a slightly different value for each satellite, due to the fit to a numerical integration. The precision on the i_j , ε_j and θ_j as given in Table 4 is 0.0001° (0.00001 rad/y and 0.001° in frequency and phase, respectively). The typical precision of the time-series for $s_{x/y}(t)$ reconstructed from Table 4 over the 1900 – 2100 interval is approximately 0.0003° (see Table 5). This corresponds to a relative truncation error below 1%. Neglecting terms related to trends would lead to typical errors of about 0.003° after 100 years in $s_{x/y}(t)$, greater than the truncation error.

For each satellite, the orbital precession is dominated by the term with $j = 1$ whose frequency corresponds to the node longitude proper frequency of that satellite. This may seem obvious, but note that this is not the case for all of the large satellites of Uranus, which strongly perturb each other [Baland et al., 2025]. The ratio i_2/i_1 is of 28%, 5%, 21%, and 12%, for Io, Europa, Ganymede, and Callisto by respectively. The dominant terms of spin precession are not necessarily the same as the dominant terms of orbital precession. The amplitude ε_j can reach a value such that θ_j is large or very small, depending on the ratio of $\omega_f/\dot{\Omega}_j$ with $\omega_f = \kappa/C$ the natural frequency of the free retrograde precession. The free mode periods are given in Table 2. In the limit case $\omega_f/\dot{\Omega}_j \rightarrow 0$ (relatively short forcing period), ε_j tends towards $-i_j$ and θ_j tends towards 0 (meaning that the spin axis tends to align with the Laplace pole, e.g. term $j = 3$ for Callisto). For $\omega_f/\dot{\Omega}_j \rightarrow \pm\infty$ (relatively long forcing period), ε_j tends towards 0 and θ_j tends towards i_j (meaning that the spin axis tends to follow the precessing orbit normal, e.g. term $j = 5$ for Io). When the ratio $\omega_f/\dot{\Omega}_j$ is close to -1 , ε_j and θ_j can be resonantly amplified (e.g. term $j = 3$ for Ganymede). The ratio θ_2/θ_1 is of 26%, 5%, 18%, 16% for Io, Europa, Ganymede and Callisto, respectively. Note that $\theta_3/\theta_1 = 22\%$ for Ganymede, while i_3/i_1 is only of 9%. The largest orbital obliquity amplitudes is ε_1 for Io, Europa and Callisto, but ε_3 for

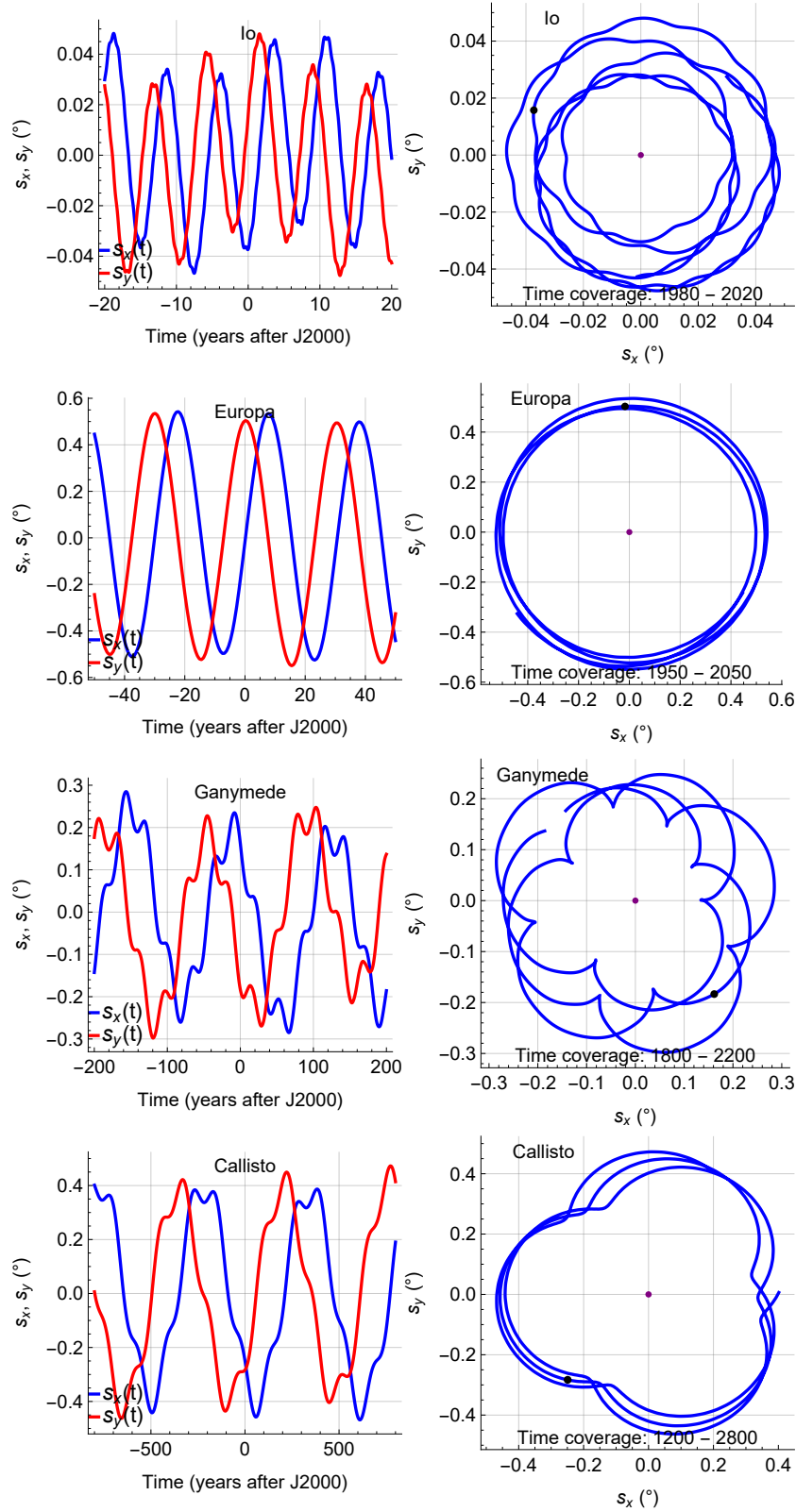


Figure 2: Temporal evolution of the spin axis coordinates in the Laplace plane s_x and s_y for the four Galilean satellites for a solid satellite. The time coverage is different for each satellite. The purple point is the Laplace pole, for which by definition $s_x = s_y = 0$. The black dots in the right graphs are the J2000 spin positions.

Ganymede. The second largest orbital obliquity amplitude is ε_4 , ε_5 , ε_1 , and ε_2 for Io, Europa, Ganymede, and Callisto, respectively.

	i_j (°)	ε_j (°)	θ_j (°)	period (y)	f_j (rad/y)	φ_j (°)	Argument	\dot{J}_{IAU}
Io								
1	0.0358	0.0020	0.0378	-7.42164	-0.84660	260.604	Ω_1	$-\dot{J}_3$
2	0.0099	0.0001	0.0100	-30.2008	-0.20805	184.095	Ω_2	$-\dot{J}_4$
3	0.0013	0.0000	0.0013	-137.325	-0.04575	59.788	Ω_3	$-\dot{J}_5$
4	0.0004	0.0006	0.0010	-0.68144	-9.22041	273.914	$-2\nu - \Omega_2$	
5	-0.0003	0.0000	-0.0003	-564.38	-0.01113	310.084	Ω_4	$-\dot{J}_6$
6	0.0003	0.0000	0.0003	5.93122	1.05934	113.504	$2L_S$	\dot{J}_8
Europa								
1	0.4651	0.0555	0.5206	-30.2008	-0.20805	184.073	Ω_2	$-\dot{J}_4$
2	0.0250	0.0006	0.0256	-137.328	-0.04575	59.767	Ω_3	$-\dot{J}_5$
3	0.0056	0.0000	0.0056	-560.607	-0.01121	310.271	Ω_4	$-\dot{J}_6$
4	-0.0012	-0.0009	-0.0021	-7.42165	-0.84660	260.589	Ω_1	$-\dot{J}_3$
5	-0.0012	0.0015	0.0003	-0.68144	-9.22041	273.897	$-2\nu - \Omega_2$	
6	0.0008	-0.0003	0.0005	5.9312	1.05934	113.500	$2L_S$	\dot{J}_8
7	0.0002	0.0001	0.0003	-11.8638	-0.52961	299.309	$-L_S$	$-\dot{J}_8/2$
8	0.0002	-0.0002	0.0000	-0.669656	-9.38270	38.1641	$-2\nu - \Omega_3$	
9	0.0001	0.0000	0.0001	11.8639	0.52961	178.045	L_S	$\dot{J}_8/2$
10	-0.0001	0.0000	-0.0001	4.95757	1.26739	68.1319	$2L_S - \Omega_2 + \Omega_0$	
Ganymede								
1	0.1860	0.0316	0.2176	-137.328	-0.04575	59.659	Ω_3	$-\dot{J}_5$
2	0.0382	0.0014	0.0396	-560.839	-0.01120	310.157	Ω_4	$-\dot{J}_6$
3	-0.0165	-0.0321	-0.0486	-30.2009	-0.20805	183.966	Ω_2	$-\dot{J}_4$
4	0.0018	-0.0014	0.0004	5.93122	1.05934	113.417	$2L_S$	\dot{J}_8
5	0.0003	-0.0007	-0.0004	-11.8633	-0.52963	298.979	$-L_S$	$-\dot{J}_8/2$
6	0.0002	-0.0002	0.0000	-0.68144	-9.22041	273.774	$-2\nu - \Omega_2$	
7	0.0002	-0.0002	0.0000	3.95426	1.58896	133.013	$3L_S$	$3\dot{J}_8/2$
8	0.0002	-0.0001	0.0001	11.8641	0.52959	177.622	L_S	$\dot{J}_8/2$
9	-0.0001	0.0001	0.0000	5.68547	1.10513	192.004	$2L_S - 2\Omega_3 + \Omega_0$	
Callisto								
1	0.2507	0.1429	0.3936	-560.826	-0.01120	309.669	Ω_4	$-\dot{J}_6$
2	-0.0302	0.0927	0.0626	-137.327	-0.04575	59.182	Ω_3	$-\dot{J}_5$
3	0.0038	-0.0037	0.0001	5.93112	1.05936	112.934	$2L_S$	\dot{J}_8
4	-0.0006	0.0007	0.0001	-30.2046	-0.20802	183.619	Ω_2	$-\dot{J}_4$
5	0.0006	-0.0006	0.0000	-11.8639	-0.52960	298.653	$-L_S$	$-\dot{J}_8/2$
6	0.0005	-0.0005	0.0000	11.865	0.52956	176.965	L_S	$\dot{J}_8/2$
7	0.0004	-0.0004	0.0000	3.95429	1.58895	132.539	$3L_S$	$3\dot{J}_8/2$
8	-0.0003	0.0003	0.0000	5.86872	1.07062	301.732	$2L_S - \Omega_4 + \Omega_0$	

Table 4: $(\Delta n_x, \Delta n_y)$ and $(\Delta s_x, \Delta s_y)$ series, according to the notations of Eqs. (48-50). Inclination, orbital and inertial obliquity amplitudes i_j , ε_j and θ_j at the frequency and phase f_j and φ_j obtained from the JUP387 orbital theory and assuming that the satellites are entirely solid and rigid. These series can be used directly to reconstruct time series for $s_{x/y}(t)$, and indirectly to reconstruct the time series for the angles $\theta(t)$, $\varepsilon(t)$, $\psi(t)$, and $\zeta(t)$ (see Section 6.2). The phases φ_j are given with respect to J2000 epoch. The last columns show the identification to the fundamental arguments of Lainey et al. [2006] and the fundamental IAU WG frequencies \dot{J}_i .

6.2 Series for obliquity, node longitude, and offset

The temporal evolution of the inertial (θ , Eq. 11a) and orbital (ε , Eq. 13) obliquities, node longitude (ψ , Eq. 11b), and offset (ζ , Eq. 16) obtained from the series of Table 3 and Table 4 are shown in Figs. 3, 4, and 5. We see that the deviation from the Cassini plane is small for Europa (usually less than 0.006°). For comparison with the spin Euler angles, the inclination (i , Eq. 12a) and orbital node longitude (Ω , Eq. 12b)

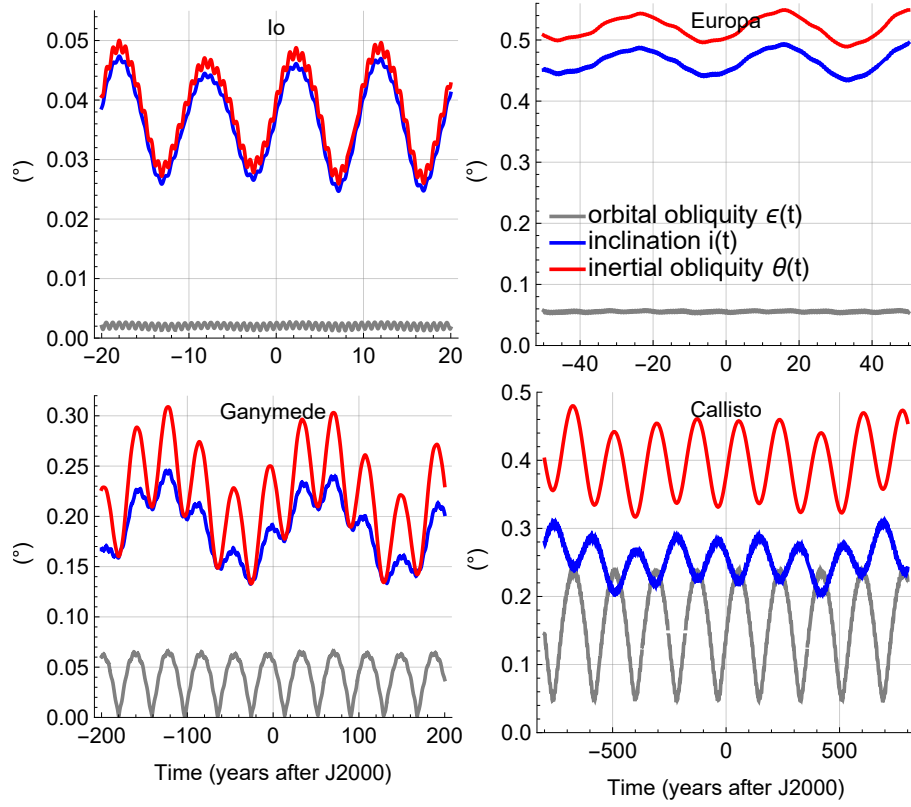


Figure 3: Temporal evolution of the orbital (ε) and inertial (θ) obliquities and of the orbital inclination (i) for the four Galilean satellites, assuming a solid interior model.

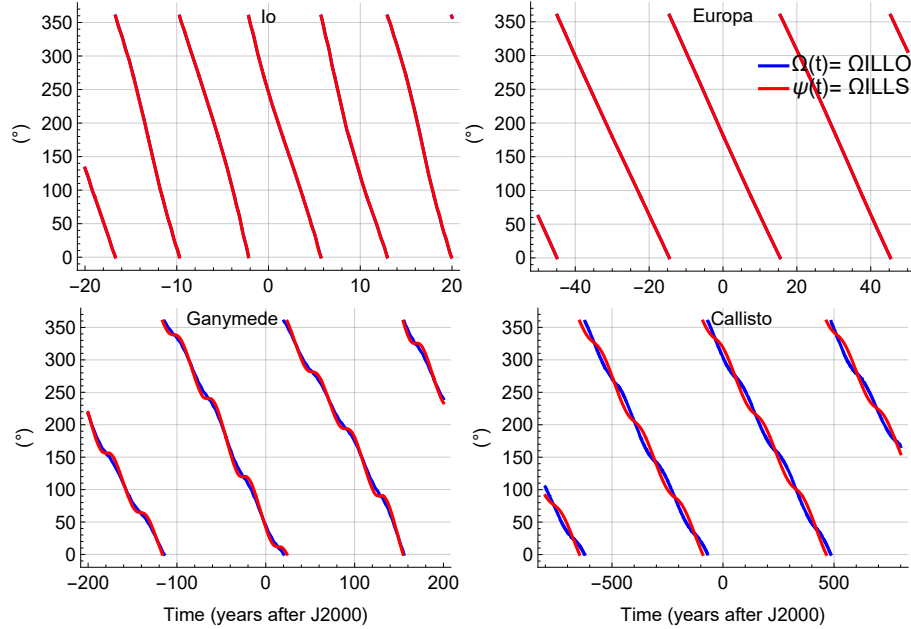


Figure 4: Node longitude of the spin (ψ) and of the orbit (Ω) as a function of time for the four Galilean satellites, assuming a solid interior model.

are also shown in Fig. 3 and 4, respectively. The typical precision (or truncation error) of the time-series $\varepsilon(t)$ and $\theta(t)$ over the 1900-2100 interval, reconstructed from Table 4, is by construction similar to that of the time-series $s_{x/y}(t)$, that is approximately 0.0003° (see Table 5). This corresponds to a relative error below 1%, except in the case of Io's orbital obliquity which is particularly small. In contrast, the longitude of

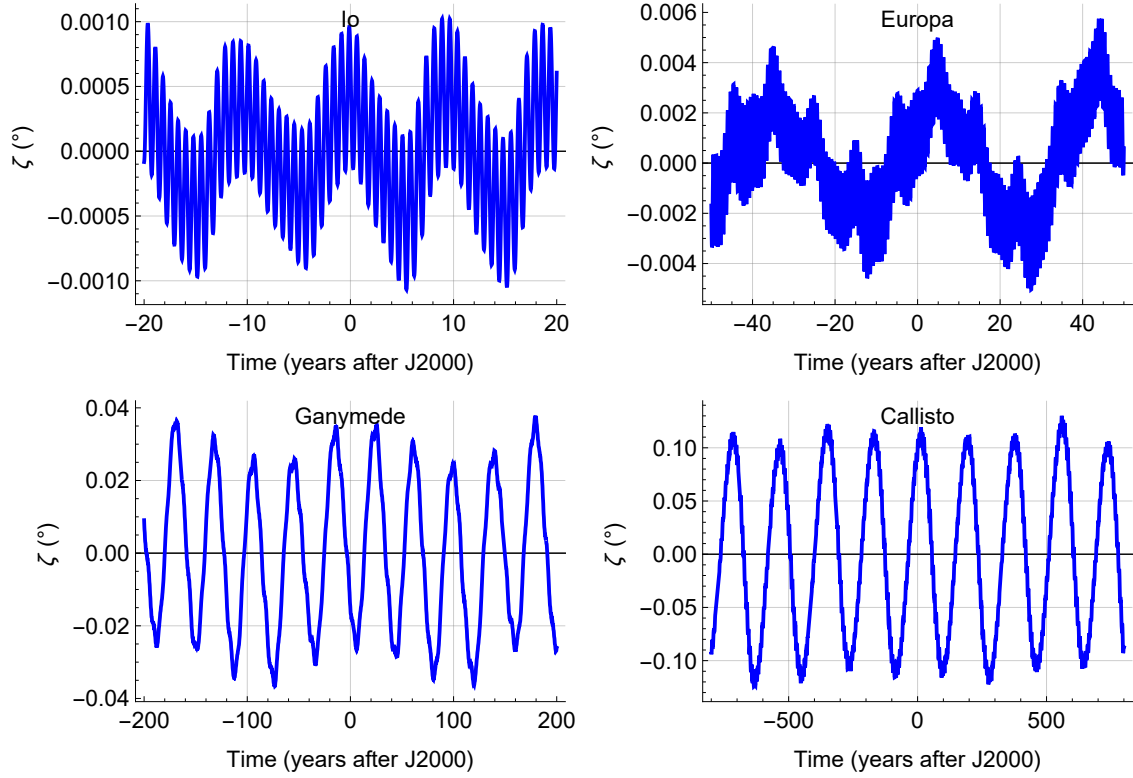


Figure 5: Offset ζ of the spin axis with respect to the Cassini plane for the four Galilean satellites, assuming a solid interior model.

the ascending node is a circulating angle, and the error associated with its reconstruction using Table 4 and Eq. (11b) is significantly larger but remains below 0.6° and therefore below the percent level. The absolute precision on the reconstructed $\zeta(t)$ is similar to that of $\varepsilon(t)$, but its relative precision may be larger than that of $\varepsilon(t)$ when the offset is small (e.g. Europa, 5%). As for $s_{x/y}(t)$, neglecting terms related to trends would lead after 100 years to typical errors larger than the truncation error in θ , ψ , and ζ (ε is not affected by the trends).

When we inject the series $(\Delta n_x, \Delta n_y)$ and $(\Delta s_x, \Delta s_y)$ from Section 6.1, Table 4, into the exact expressions for θ (Eq. 11a), ψ (Eq. 11b), ε (Eq. 15a), and ζ (Eq. 16) given in Sections 3.3 and 3.4, we obtain expressions which do not have the form of a periodic series. Periodic series can be obtained instead by developing the angles' expressions of Eqs. (14a, 14c, 15a, 17a) around the dominant terms of the series $(\Delta n_x, \Delta n_y)$ and $(\Delta s_x, \Delta s_y)$, when they exist. If the first periodic term (with amplitudes i_1 , θ_1 and ε_1) dominates the other periodic terms (i_j , θ_j and ε_j with $j > 1$) and considering that the trends tr_x and tr_y are small, we can write the following developments for the inertial and orbital obliquities, the node longitude and the offset from

	s_x, s_y (10^{-4}° / %)	θ (10^{-4}° / %)	ψ ($^\circ$ / %)	ε (10^{-4}° / %)	ζ (10^{-4}° / %)
Truncation error of Table 4					
Io	3 / 0.6	3 / 0.6	0.6 / 0.15	2 / 6	2 / 10
Europa	4 / 0.06	3 / 0.04	0.04 / 0.01	2 / 0.4	3 / 5
Ganymede	2 / 0.08	2 / 0.06	0.06 / 0.02	3 / 0.6	3 / 1
Callisto	2 / 0.04	2 / 0.03	0.03 / 0.01	2 / 0.1	4 / 0.4
Development error					
Io (order 3)	-	2 / 0.3	0.4 / 0.1	< 1 / 0.1	< 1 / 2
Europa (order 2)	-	< 1 / < 0.1	0.01 / 0.01	< 1 / < 0.1	< 1 / 0.2
Ganymede (order 5)	-	1 / < 0.1	0.5 / 0.2	60 / 9	< 1 / 0.1
Callisto (order 5)	-	< 1 / < 0.1	0.01 / 0.01	10 / 0.4	< 1 / < 0.1
Error after 100 years if the linear/Poisson terms are neglected					
Io	30 / 0.05	40 / 7	7 / 2	-	3 / 30
Europa	30 / 0.5	35 / 0.6	0.3 / 0.1	-	4 / 7
Ganymede	30 / 0.3	30 / 1	2 / 0.6	-	8 / 2
Callisto	30 / 0.4	40 / 1	0.4 / 0.1	-	20 / 2

Table 5: Comparison of different errors affecting the angles over the 1900-2100 period. The first source of error arises from the truncation applied in Table 4. Each term in the $s_{x/y}$ series is truncated at a level of 0.0001° in amplitude, which is also the truncation threshold applied to the series. The cumulative errors on $s_{x/y}(t)$, and therefore on $\theta(t)$, $\varepsilon(t)$, and $\zeta(t)$, lead to a total truncation error of about 0.0003° . The cumulative truncation errors on the node longitude ψ reach up to 0.6° for Io. The second source of error is the development error, arising when θ , ψ , ε , and ζ are developed as series themselves. A third possible source of error stems from the omission of the linear and Poisson terms.

the Cassini plane, up to order 2 in the small amplitudes of the other terms and in the trends:

$$\begin{aligned} \theta(t) \approx & \theta_1 + (tr_x \sin \xi_1 - tr_y \cos \xi_1) t - (tr_x \cos \xi_1 + tr_y \sin \xi_1) t \sum_{j=2}^N \frac{\theta_j}{\theta_1} \sin(\xi_1 - \xi_j) \\ & + \sum_{j=2}^N \theta_j \cos(\xi_1 - \xi_j) + \sum_{k=2}^N \sum_{j=2}^N \frac{\theta_k \theta_j}{2 \theta_1} \sin(\xi_1 - \xi_k) \sin(\xi_1 - \xi_j), \end{aligned} \quad (51a)$$

$$\begin{aligned} \psi(t) \approx & \xi_1 + \frac{1}{\theta_1} (tr_x \cos \xi_1 + tr_y \sin \xi_1) t - t \sum_{j=2}^N \frac{\theta_j}{\theta_1^2} (tr_x \cos(2\xi_1 - \xi_j) + tr_y \sin(2\xi_1 - \xi_j)) \\ & - \sum_{j=2}^N \frac{\theta_j}{\theta_1} \sin(\xi_1 - \xi_j) + \sum_{k=2}^N \sum_{j=2}^N \frac{\theta_k \theta_j}{\theta_1^2} \cos(\xi_1 - \xi_k) \sin(\xi_1 - \xi_j), \end{aligned} \quad (51b)$$

$$\varepsilon(t) \approx \varepsilon_1 + \sum_{j=2}^N \varepsilon_j \cos(\xi_1 - \xi_j) + \sum_{k=2}^N \sum_{j=2}^N \frac{\varepsilon_k \varepsilon_j}{2 \varepsilon_1} \sin(\xi_1 - \xi_k) \sin(\xi_1 - \xi_j), \quad (51c)$$

$$\begin{aligned} \zeta(t) \approx & -(tr_x \cos \xi_1 + tr_y \sin \xi_1) \frac{\varepsilon_1}{i_1} t \\ & + t \sum_{j=2}^N \left(\frac{2\varepsilon_1 i_j - i_1 \varepsilon_j}{2i_1^2} (tr_x \cos(2\xi_1 - \xi_j) + tr_y \sin(2\xi_1 - \xi_j)) - \frac{i_1 \varepsilon_j}{2i_1^2} (tr_x \cos \xi_j + tr_y \sin \xi_j) \right) \\ & + \sum_{j=2}^N \frac{\varepsilon_1 i_j - \varepsilon_j i_1}{i_1} \sin(\xi_1 - \xi_j) + \sum_{k=2}^N \sum_{j=2}^N \frac{i_j (\varepsilon_k i_1 - \varepsilon_1 i_k)}{i_1^2} \cos(\xi_1 - \xi_k) \sin(\xi_1 - \xi_j), \end{aligned} \quad (51d)$$

where we use the notation $\xi_j = f_j t + \varphi_j$. i_j , ε_j , θ_j , f_j , and φ_j are given in columns 3, 4, 6, and 7 in Table 4. As already noted after Eq. (15a), ε is unaffected by the long-term trends. Developments of a higher order are usually necessary to reach a sufficient accuracy in the time domain.

Note that the presence, absence, or even the position in the series of a single dominant term, when it exists, may change significantly when considering a different interior model than the solid one used here. Some amplitudes may be amplified or diminished, resulting in a markedly different configuration.

	$\mathcal{E}_j (^{\circ})$	$\mathcal{Z}_j (^{\circ})$	period (y)	f_j (rad/y)	$\varphi_j (^{\circ})$	Argument
Io	$\mathcal{E}_{cst} = 0.0020$					
1	0.0006	0.0006	-0.75034	-8.37381	13.310	$-2\nu - \Omega_1 - \Omega_2$
2	0.0001	0.0005	-9.83977	-0.63855	76.509	$\Omega_1 - \Omega_2$
Europa	$\mathcal{E}_{cst} = 0.0555$					
1	0.0015	0.0016	-0.69717	-9.01236	89.824	$-2\nu - 2\Omega_2$
2	-0.0009	-0.0008	-9.83977	-0.63855	76.516	$\Omega_1 - \Omega_2$
3	0.0006	0.0024	-38.7134	-0.1623	124.306	$\Omega_2 - \Omega_3$
4	0.0000	-0.0007	31.9203	0.19684	126.198	$-\Omega_2 + \Omega_4$
Ganymede	$\mathcal{E}_{cst} = 0.0403$					
1	-0.0279	-0.0293	-38.7134	-0.16230	124.307	$\Omega_2 - \Omega_3$
2	-0.0060	-0.0013	-19.3567	-0.32460	248.614	$2\Omega_2 - 2\Omega_3$
3	-0.0041	0.0000	-12.9045	-0.48690	12.921	$3\Omega_2 - 3\Omega_3$
4	-0.0026	0.0000	-9.67835	-0.64920	137.228	$4\Omega_2 - 4\Omega_3$
5	-0.0010	-0.0017	5.68568	1.10509	53.758	$2L_S - \Omega_3$
6	0.0010	-0.0051	181.858	0.03455	250.498	$-\Omega_3 + \Omega_4$
7	-0.0008	0.0032	31.9186	0.19685	126.191	$-\Omega_2 + \Omega_4$
8	0.0008	-0.0002	-4.95758	-1.26739	70.549	$\Omega_2 - 2L_S$
9	0.0004	0.0028	-49.1834	-0.12775	14.805	$\Omega_2 - 2\Omega_3 + \Omega_4$
10	-0.0005	-0.0008	-12.985	-0.48388	239.320	$-\Omega_3 - L_S$
Callisto	$\mathcal{E}_{cst} = 0.1584$					
1	0.0875	-0.1100	181.858	0.03455	250.487	$-\Omega_3 + \Omega_4$
2	-0.0133	-0.0066	90.9289	0.06910	140.974	$-2\Omega_3 + 2\Omega_4$
3	0.0042	0.0000	60.6193	0.10365	31.461	$3\Omega_4 - 3\Omega_3$
4	-0.0033	0.0059	-5.86906	-1.07056	196.735	$\Omega_4 - 2L_S$
5	-0.0017	0.0000	45.4644	0.13820	281.948	$4\Omega_4 - 4\Omega_3$
6	-0.0013	-0.0005	5.68557	1.10511	53.752	$2L_S - \Omega_3$
7	0.0010	0.0012	-6.06479	-1.03601	87.222	$-\Omega_3 + 2\Omega_4 - 2L_S$
8	0.0009	0.0000	36.3716	0.17275	172.435	$5\Omega_4 - 5\Omega_3$
9	0.0006	-0.0010	31.9235	0.19682	126.050	$-\Omega_2 + \Omega_4$
10	-0.0005	0.0009	12.1203	0.51840	11.016	$\Omega_4 + L_S$
11	-0.0005	0.0000	-6.27403	-1.00146	337.709	$-2\Omega_3 + 3\Omega_4 - 2L_S$
12	-0.0004	0.0008	-11.6192	-0.54076	132.704	$\Omega_4 - L_S$
13	-0.0004	0.0006	-3.92662	-1.60015	177.130	$\Omega_4 - 3L_S$
14	0.0003	-0.0005	-5.80798	-1.08182	7.937	$2\Omega_4 - \Omega_0 - 2L_S$

Table 6: Periodic development of the orbital obliquity ε and the Cassini plane offset ζ for the four Galilean satellites, considered as solid. We consider developments up to orders 3, 2, 5, and 5, for Io, Europa, Ganymede, and Callisto, respectively. The series presented in this table are provided for illustrative purposes, with the smallest terms omitted for the sake of brevity. For each satellite, the first term of the obliquity is the constant mean value \mathcal{E}_{cst} . The phases φ_j are given with respect to J2000 epoch.

If the first, second, and possibly higher order terms are combined into pure trigonometric terms, each

development can then be written as a trigonometric series:

$$\theta(t) \approx \mathcal{T}_{cst} + \sum_j \mathcal{T}_j \cos \xi_j + t \sum_k (\mathcal{T}_k^c \cos \xi_k + \mathcal{T}_k^s \sin \xi_k), \quad (52a)$$

$$\psi(t) \approx \xi_1 + \sum_j \mathcal{P}_j \sin \xi_j + t \sum_k (\mathcal{P}_k^c \cos \xi_k + \mathcal{P}_k^s \sin \xi_k), \quad (52b)$$

$$\varepsilon(t) \approx \mathcal{E}_{cst} + \sum_j \mathcal{E}_j \cos \xi_j, \quad (52c)$$

$$\zeta(t) \approx \sum_j \mathcal{Z}_j \sin \xi_j + t \sum_k (\mathcal{Z}_k^c \cos \xi_k + \mathcal{Z}_k^s \sin \xi_k). \quad (52d)$$

The general form of these expansions remains valid for developments at any order. The series expansions for θ and ε contain a mean term, \mathcal{T}_{cst} and \mathcal{E}_{cst} , respectively, which differ from θ_1 and ε_1 for high order developments, while the mean Cassini plane offset value is zero. The first term of ψ is ξ_1 , the first argument of the n/s series. Each angle has a periodic cosine or sine series. Except for ε , all angles have a Poisson series with both cosine and sine amplitudes multiplied by the time t . The arguments of the periodic and Poisson series are always a linear combination of ξ_j arguments of Table 4.

These trigonometric developments can be very accurate. If we go up to orders 3, 2, 5, and 5 respectively, for each satellite, the "development error" is usually less than 1%, except for the orbital obliquity of Ganymede (9%, see Table 5). Considering a higher order for Ganymede's ε does not solve the accuracy issue, as the development cannot converge due to $|\varepsilon_1/\varepsilon_3| \sim 1$. For Europa, it is possible to neglect the second-order terms of the development while maintaining a reasonable accuracy (e.g. 10^{-4}° or about 0.2% in ε). Compared with a purely numerical solution obtained from ephemerides, these development errors should be added to the truncation errors in the original series in n/s , discussed in Section 6.1 and summarized in the first four lines of Table 5, to obtain the total error budget.

We do not show the trigonometric expansions here in their entirety, as they can include dozens and dozens of terms. For illustration purposes only, we provide truncated, and therefore imprecise, expansions in Tables 6 to 8, for the periodic and Poisson terms. At least as far as the most important terms are concerned, the θ and ψ series, as well as the ε and ζ series, tend to contain terms with the same arguments. The series for ψ are multiplied by θ_1 to obtain amplitudes of the same order as those of θ . The Poisson series for the angles ψ , θ and ζ are plotted on Fig. 6. Between 2030 and 2035, during the JUICE mission timeframe, Ganymede's Poisson terms can reach approximately up to 0.001° , 1° , and 0.0005° for θ , ψ , and ζ , respectively. The periodic series of the orbital obliquity for Callisto closely matches the solution of Noyelles [2009] (see his Table 10), which was derived through frequency decomposition of a numerical integration of the Hamiltonian equations. Differences in amplitudes and frequencies are generally within a few percent, and are probably partly due to the use of a different ephemeris. This comparison of our analytical results and this numerical series provides support for our approach. A key advantage of our method is its ability to clearly identify the various contributing terms, including the Poisson terms.

For Io and Europa, $\mathcal{T}_{cst} \sim \theta_1$ and $\mathcal{E}_{cst} \sim \varepsilon_1$, while most of their periodic terms are such that $|\mathcal{T}_j| \sim |\theta_1 \mathcal{P}_j| \sim |\theta_j|$ as can be understood from the first-order term in Eq. (51a). Note, however, that the argument of each term is now a combination of two distinct arguments, rather than the original single argument of Table 4, so the periodicity will be different from the s_x/s_y series. Most of their amplitudes \mathcal{E}_j are also obtained essentially as first-order terms in Eq. (51c) and therefore tend to be similar to the amplitudes ε_j , but are not organized in the same order. For those first order terms, \mathcal{Z}_j are not expected to be similar to ε_j , however, see Eq. (51d). For Ganymede (Callisto), because of the relatively large amplitudes of the second and third terms (second term) in Table 4, the amplitudes in Tables 7 and 6 do not necessarily correspond to those in Table 4 (especially for ε in the case of Ganymede) and there are many high-order terms involved.

With the exception of the orbital obliquity of Ganymede, the series of θ , ψ , ε , and ζ help us to understand the temporal behavior of these angles (Figs. 2, 3, 4, and 5). The second terms of the series perturb the inertial obliquity of Io, Europa, Ganymede and Callisto by 26%, 5%, 22%, and 16%, respectively. The third term of Ganymede's series perturbs its inertial obliquity by 18%, see third panel of Fig. 3. The main perturbation of ε comes from \mathcal{E}_1 which is similar (or at least mainly originates from) to ε_4 , ε_5 , and ε_2 for Io, Europa, and Callisto, respectively. Europa's orbital obliquity varies by 3% over time, while its spin axis describes an

almost circular trajectory in space, see Fig. 2. For Io and Callisto, ε varies by 30% and 55%, respectively. For Ganymede, ε varies by almost 100% around its mean value, between 0 and 0.6° , but this is poorly described by the ε series. Callisto has the largest offset of the four satellites. Its periodic variations are dominated by the first term of the offset series with an amplitude $\mathcal{Z}_1 = 0.11^\circ$.

	\mathcal{T}_j ($^\circ$)	$\theta_1 \mathcal{P}_j$ ($^\circ$)	period (y)	f_j (rad/y)	φ_j ($^\circ$)	Argument
Io	$\mathcal{T}_{cst} = 0.0385$					
1	0.0099	-0.0100	-9.83977	-0.63855	76.509	$\Omega_1 - \Omega_2$
2	0.0013	-0.0013	-7.84565	-0.80085	200.816	$\Omega_1 - \Omega_3$
3	0.0010	0.0010	-0.75034	-8.37381	13.310	$-2\nu - \Omega_1 - \Omega_2$
4	-0.0007	0.0014	-4.92655	-1.27537	146.715	$2\Omega_1 - 2\Omega_2$
Europa	$\mathcal{T}_{cst} = 0.5209$					
1	0.0256	-0.0256	-38.7134	-0.16230	124.306	$\Omega_2 - \Omega_3$
2	0.0056	0.0056	31.9203	0.19684	126.198	$-\Omega_2 + \Omega_4$
3	-0.0021	-0.0021	-9.83977	-0.63855	76.516	$\Omega_1 - \Omega_2$
4	0.0005	-0.0005	-4.95758	-1.26739	70.573	$\Omega_2 - 2L_S$
Ganymede	$\mathcal{T}_{cst} = 0.2222$					
1	-0.0479	-0.0486	-38.7134	-0.1623	124.307	$\Omega_2 - \Omega_3$
2	0.0389	0.0396	181.858	0.03455	250.498	$-\Omega_3 + \Omega_4$
3	-0.0045	0.0000	31.9186	0.19685	126.191	$-\Omega_2 + \Omega_4$
4	0.0043	0.0088	-49.1834	-0.12775	14.805	$\Omega_2 - 2\Omega_3 + \Omega_4$
5	-0.0026	-0.0054	-19.3567	-0.3246	248.614	$2\Omega_2 - 2\Omega_3$
6	-0.0017	-0.0036	90.9289	0.0691	140.996	$-2\Omega_3 + 2\Omega_4$
7	0.0007	0.002	-21.6624	-0.29005	139.112	$2\Omega_2 - 3\Omega_3 + \Omega_4$
8	-0.0006	-0.0016	-67.4162	-0.0932	265.303	$\Omega_2 - 3\Omega_3 + 2\Omega_4$
Callisto	$\mathcal{T}_{cst} = 0.3961$					
1	0.0624	-0.0626	181.858	0.03455	250.487	$-\Omega_3 + \Omega_4$
2	-0.0025	0.005	90.9289	0.0691	140.974	$-2\Omega_3 + 2\Omega_4$

Table 7: Periodic development of the inertial obliquity θ and the node longitude ψ for the four Galilean satellite, considered as solid. We consider developments up to orders 3, 2, 5, and 5, for Io, Europa, Ganymede, and Callisto, respectively. The series presented in this table are provided for illustrative purposes, with the smallest terms omitted for the sake of brevity. For each satellite, the first term of the inertial obliquity is the constant mean value \mathcal{T}_{cst} . The phases φ_j are given with respect to J2000 epoch.

	\mathcal{T}_j^c	\mathcal{T}_j^s	$\theta_1 \mathcal{P}_j^c$	$\theta_1 \mathcal{P}_j^s$	\mathcal{Z}_j^c	\mathcal{Z}_j^s	period (y)	f_j (rad/y)	φ_j ($^\circ$)	Argument
Io										
1	-24	-27	-28	24	2	-1	-7.42167	-0.8466	260.604	Ω_1
2	4	4	7	-6	0	0	-4.23067	-1.48515	337.113	$2\Omega_1 - \Omega_2$
Europa										
1	-24	-28	-28	24	3	-3	-30.2004	-0.20805	184.073	Ω_2
Ganymede										
1	-23.	-27	-28	24	5	-4	-137.337	-0.04575	59.659	Ω_3
2	-3.	-3	-6	5	-2	2	53.8619	0.11665	296.538	$2\Omega_3 - \Omega_2$
Callisto										
1	-25.	-28	-28	25	16	-15	-560.999	-0.0112	309.669	Ω_4
2	2.	2	5	-4	0	0	269.67	0.0233	199.92	$2\Omega_4 - \Omega_3$

Table 8: Poisson series for the angles θ , ψ and ζ , including cosine and sine terms. Amplitude units are $10^{-6}^\circ/\text{y}$. The phases φ_j are given with respect to J2000 epoch.

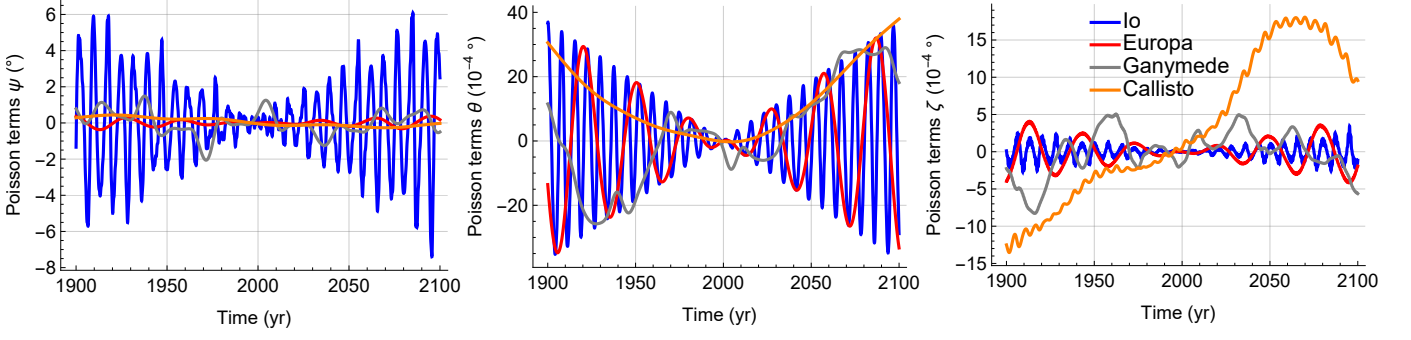


Figure 6: Poisson terms for the angles ψ , θ and ζ for the four Galilean satellites over the calendar period 1900-2100.

6.3 Series for (α_S, δ_S) and W

We assume for α_S and δ_S a form similar to that of s_x and s_y , but with non-zero mean terms:

$$\alpha_S(t) = \alpha_{LP} + tr_\alpha t + \sum_j \alpha_j^S \sin(f_j t + \varphi_j), \quad (53a)$$

$$\delta_S(t) = \delta_{LP} + \delta_{S0} + tr_\delta t + \sum_j \delta_j^S \cos(f_j t + \varphi_j). \quad (53b)$$

The mean value of α_S is that of the Laplace plane (α_{LP}), as already noticed in Eq. (7), see Section 3. For δ_S , the mean value is the sum of δ_{LP} and of $\delta_{S0} \sim \theta_1^2 \tan \delta_{LP}/4$, the latter being a small increment due to the power reduction of a squared sine term in the second-order part of Eq. (8b). As part of the transformation, this incremental quantity depends on the assumed interior model for the satellites (for instance, entirely solid or not). For W , we reexpress Eq. (31) assuming the following form:

$$W = W_0 + \dot{W}t + \gamma_u + \sum_j \mu_j \sin(f_j t + \varphi_j), \quad (54)$$

where \dot{W} is defined as $n_L + tr_\mu$, see Eq. (32), with tr_μ the rate in angle μ . γ_u is the libration angle defined with respect to a uniform rotation, see Eq. (27a). The last term is the series $\Delta\mu$ expressed in a form similar to that of $\Delta s_{x/y}$.

Using the transformations of Eqs. (8), (10), and (23) on the spin model developed in Section 6.1, we find values for the rates and for the amplitudes of the periodic series in α , δ and μ , as well as for the increment δ_{S0} , see Tables 3 and 9. δ_{S0} ranges from -10^{-5} deg for Io to $-2.5 \cdot 10^{-3}$ deg for Europa, see Table 3, which have respectively the smallest and largest dominant inertial obliquity amplitude θ_1 . Figure 7 shows the temporal evolution of the right ascension α_S and declination δ_S angles, whereas the evolution of μ is presented in Fig. 8.

The chosen truncation level of the Table 9 is 0.0001° on the δ_j^S individual amplitudes. The last columns show the identification to the fundamental arguments of Lainey et al. [2006] and to the IAU WG frequencies. The J_i frequencies appearing in Archinal et al. [2018] are indicated in bold: 2 lines for Io, 4 for Europa and 3 for Ganymede and Callisto. Even though the frequencies and phases of the fundamental arguments are not affected by the transformation, the second order terms of the transformation give rise to new argument combinations in Table 9, labeled with the symbol $O2$, compared to Table 4, see for instance the term with argument $2\Omega_2$ for Europa, already present in Archinal et al. [2018] after Lieske [1979] (see his Eq. 18). Because of the truncation levels and of second-order terms, the number of terms for Europa, Ganymede and Callisto differ from the number of terms retained in Table 4 in the first place. For Io, all the second order terms are below the truncation level and each term in Table 9 corresponds to the original term in Table 4. For the k^{th} satellite, the $\Delta\alpha_S$, $\Delta\delta_S$, and $\Delta\mu$ series are dominated by the Ω_k term.

We now compare in the time domain the approximate series of Table 9 for α_S and δ_S to their exact transformation from Table 4 and Eqs. (5a)-(5b). Depending on whether or not the second-order transformation

	α_j^S (°)	δ_j^S (°)	μ_j (°)	period (y)	f_j (rad/y)	φ_j (°)	Argument	\dot{J}_{IAU}
Io								
1	0.0878	-0.0378	-0.0793	-7.42164	-0.84660	260.604	Ω_1	$-\dot{J}_3$
2	0.0233	-0.0100	-0.0210	-30.2008	-0.20805	184.095	Ω_2	$-\dot{J}_4$
3	0.0030	-0.0013	-0.0027	-137.325	-0.04575	59.788	Ω_3	$-\dot{J}_5$
4	0.0023	-0.0010	-0.0021	-0.68144	-9.22041	273.914	$-2\nu - \Omega_2$	
5	-0.0008	0.0003	0.0007	-564.38	-0.01113	310.084	Ω_4	$-\dot{J}_6$
6	0.0006	-0.0003	-0.0006	5.93122	1.05934	113.504	$2L_S$	\dot{J}_8
Europa								
1	1.2097	-0.5206	-1.0920	-30.2008	-0.20805	184.073	Ω_2	$-\dot{J}_4$
2	0.0595	-0.0256	-0.0537	-137.328	-0.04575	59.767	Ω_3	$-\dot{J}_5$
3	0.0131	-0.0056	-0.0118	-560.607	-0.01121	310.271	Ω_4	$-\dot{J}_6$
4 (O2)	-0.0115	0.0025	0.0116	-15.1004	-0.41609	8.146	$2\Omega_2$	$-\dot{J}_7 = -2\dot{J}_4$
5	-0.0049	0.0021	0.0044	-7.42165	-0.84660	260.589	Ω_1	$-\dot{J}_3$
6	0.0013	-0.0005	-0.0011	5.9312	1.05934	113.500	$2L_S$	\dot{J}_8
7	0.0007	-0.0003	-0.0007	-0.68144	-9.22041	273.897	$-2\nu - \Omega_2$	
8	0.0007	-0.0003	-0.0006	-11.8638	-0.52961	299.309	$-L_S$	$-\dot{J}_8/2$
9 (O2)	0.0000	-0.0002	0.0000	-38.7149	-0.16229	124.306	$\Omega_2 - \Omega_3$	$-\dot{J}_4 + \dot{J}_5$
10 (O2)	-0.0011	0.0002	0.0011	-24.7564	-0.25380	243.840	$\Omega_2 + \Omega_3$	$-\dot{J}_4 - \dot{J}_5$
Ganymede								
1	0.5066	-0.2176	-0.4575	-137.328	-0.04575	59.659	Ω_3	$-\dot{J}_5$
2	-0.1132	0.0486	0.1022	-30.2009	-0.20805	183.966	Ω_2	$-\dot{J}_4$
3	0.0922	-0.0396	-0.0833	-560.839	-0.01120	310.157	Ω_4	$-\dot{J}_6$
4 (O2)	-0.0020	0.0004	0.0020	-68.664	-0.09151	119.318	$2\Omega_3$	$-2\dot{J}_5$
5	-0.0010	0.0004	0.0009	-11.8633	-0.52963	298.979	$-L_S$	$-\dot{J}_8/2$
6	0.0010	-0.0004	-0.0009	5.93122	1.05934	113.417	$2L_S$	\dot{J}_8
7 (O2)	-0.0000	0.0002	0.0000	-38.715	-0.16229	124.307	$\Omega_2 - \Omega_3$	$-\dot{J}_4 + \dot{J}_5$
8 (O2)	0.0009	-0.0002	-0.0009	-24.7565	-0.25380	243.626	$\Omega_2 + \Omega_3$	$-\dot{J}_4 - \dot{J}_5$
9 (O2)	0.0000	-0.0002	0.0000	181.858	0.03455	250.498	$-\Omega_3 + \Omega_4$	$\dot{J}_5 - \dot{J}_6$
10 (O2)	-0.0007	0.0002	0.0007	-110.316	-0.05696	9.816	$\Omega_3 + \Omega_4$	$-\dot{J}_5 - \dot{J}_6$
Callisto								
1	0.9253	-0.3936	-0.8374	-560.826	-0.01120	309.668	Ω_4	$-\dot{J}_6$
2	0.1470	-0.0626	-0.1331	-137.327	-0.04575	59.182	Ω_3	$-\dot{J}_5$
3 (O2)	-0.0068	0.0014	0.0068	-280.413	-0.02241	259.337	$2\Omega_4$	$-2\dot{J}_6$
4 (O2)	0.0000	-0.0005	0.0000	181.858	0.03455	250.487	$-\Omega_3 + \Omega_4$	$\dot{J}_5 - \dot{J}_6$
5 (O2)	-0.0022	0.0005	0.0022	-110.315	-0.05696	8.850	$\Omega_3 + \Omega_4$	$-\dot{J}_5 - \dot{J}_6$
6	0.0003	-0.0001	-0.0002	5.93112	1.05936	112.934	$2L_S$	\dot{J}_8

Table 9: Spin variations series $\Delta\alpha_S$, $\Delta\delta_S$ and $\Delta\mu$ of the Galilean satellites for the solid interior model and the JUP387 orbital theory. The truncation level is 0.0001° on the δ_j^S amplitudes. The last columns show the identification to the fundamental arguments of Lainey et al. [2006] and to the IAU WG frequencies \dot{J}_i . The \dot{J}_i frequencies appearing in Archinal et al. [2018] are indicated in bold. Second order terms, not present in the $\Delta s_{x/y}$ series, are labeled with the symbol O2. These series can be used to reconstruct time series for $\alpha/\delta_S(t)$ and $\mu(t)$, and indirectly to reconstruct the time series for the angles $\theta(t)$, $\varepsilon(t)$, $\psi(t)$, and $\zeta(t)$. The phases φ_j are given with respect to J2000 epoch.

terms of Eqs. (8) are used or not, the error is generally less than 0.0002° or 0.02° , respectively, see Table 10 for the Galilean satellites assumed to be entirely solid. For $\mu = \beta - \psi$, the comparison between the approximate series of Table 9 and the exact transformation of Eqs. (11b, 21) indicates an accuracy generally better than 0.0002° or 0.013° for the second or first-order transformations, respectively, see Table 10. Compared with a purely numerical solution obtained from ephemerides, these transformation errors should be added to the truncation errors in the original series in n/s , see Table 5, to obtain the total error budget. Neglecting

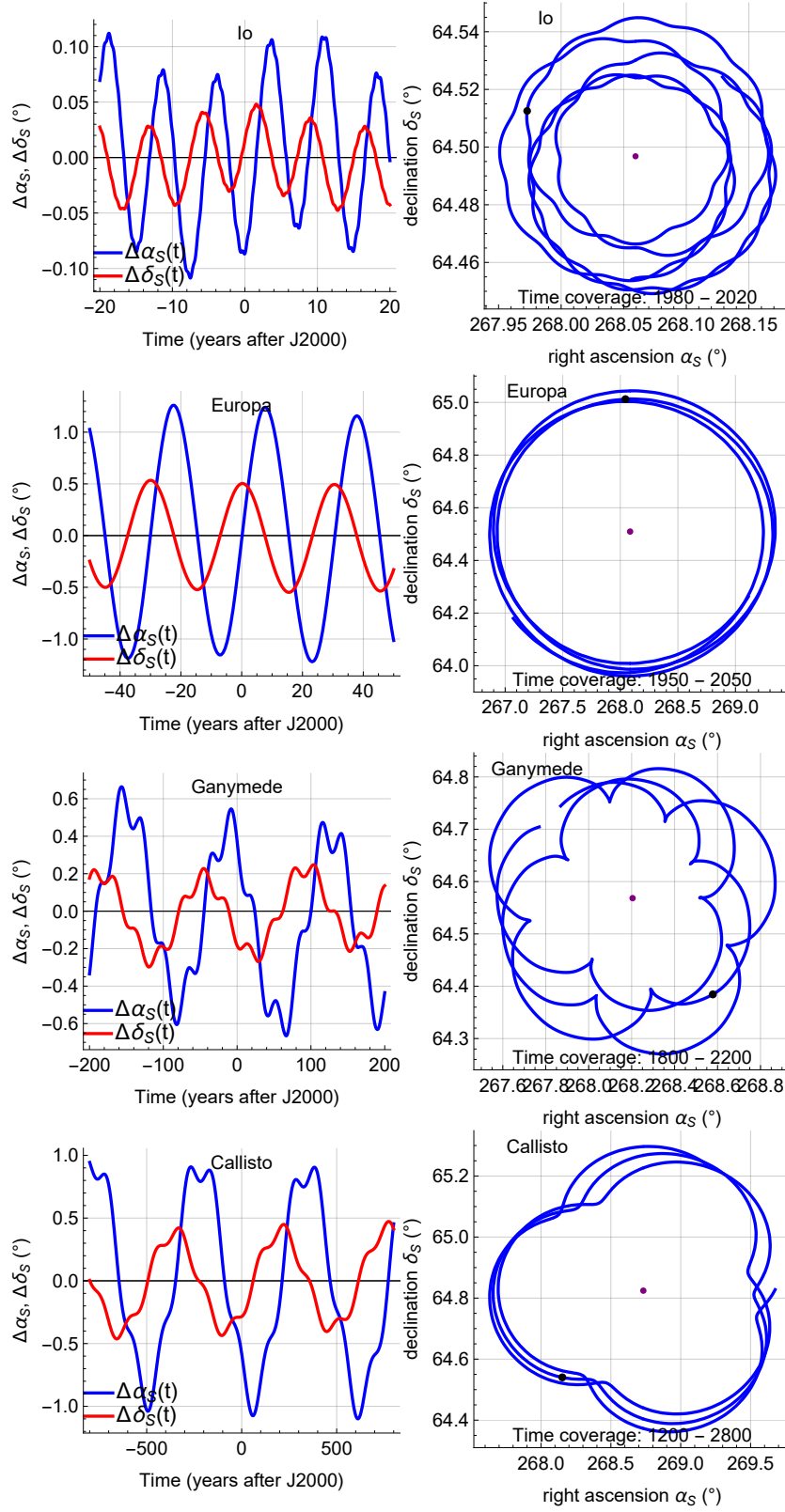


Figure 7: Temporal evolution of the spin axis angle (right ascension α_S and declination δ_S) for the four Galilean satellites. The left plot show the periodic variations while the right plot shows the projection of the motion in the ICRF plane for a solid satellite. The purple point is the Laplace plane (α_{LP}, δ_{LP}) while the black dot is the J2000 spin position.

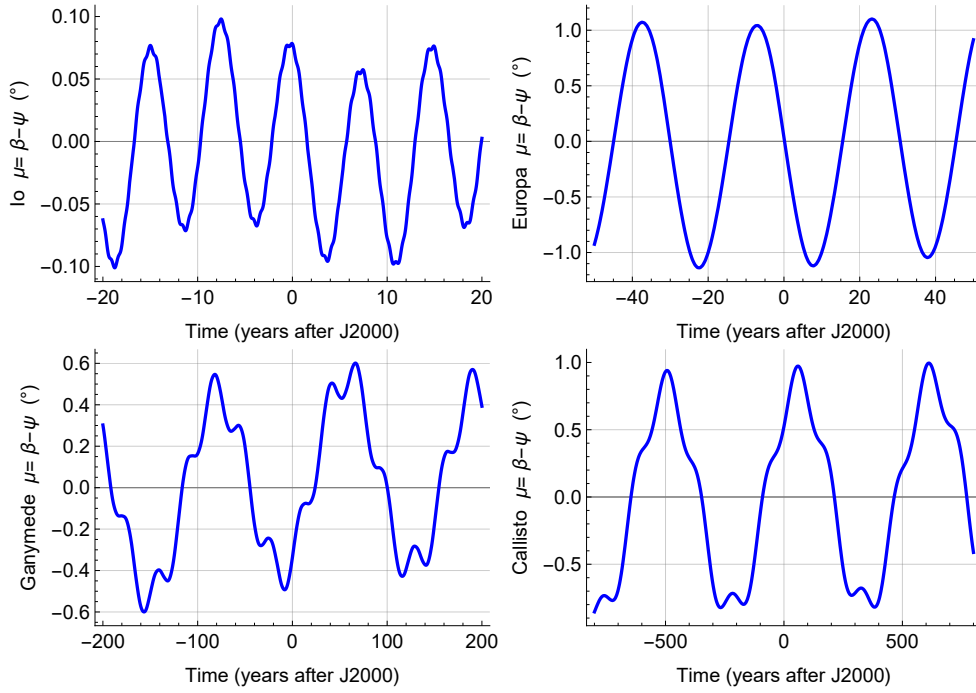


Figure 8: Temporal evolution of the μ angle ($\mu = \beta - \psi$) for the four Galilean satellites, assuming a solid interior model.

secular terms would lead to typical errors of about 0.007° , 0.003° , and 0.006° after 100 years in α_S , δ_S , and μ , respectively, larger than the combined truncation and second-order transformation errors.

Starting from the periodic series $\Delta\alpha_S$ and $\Delta\delta_S$ and Eqs. (14b, 14d, 15b, 17b), it is possible to obtain periodic series for the angles θ , ε , ψ and ζ . We do not carry out this exercise here, as it would be very similar to the one based on the series $\Delta n_{x/y}$ and $\Delta s_{s/y}$, see Section 6.2.

Errors ($^\circ$)	α_S		δ_S		μ	
	1st order	2nd order	1st order	2nd order	1st order	2nd order
Io	0.0001	0.0001	0.0000	0.0000	0.0001	0.0000
Europa	0.0131	0.0005	0.0056	0.0001	0.0132	0.0002
Ganymede	0.0038	0.0001	0.0015	0.0001	0.0037	0.00003
Callisto	0.0090	0.0003	0.0039	0.0001	0.0094	0.0001

Table 10: Maximal value of the errors of the first and second order estimations (in degree) for the four Galilean satellites for the spin right ascension α_S , the declination δ_S and the angle μ for a solid satellite.

7 Recommendations for updating the IAU WGCCRE model

The IAU Working Group on Cartographic Coordinates and Rotational Elements (WGCCRE) provides rotational elements of the planets and satellites, describing the direction of the North pole of rotation and the position of the prime meridian, see Archinal et al. [2018] for the last report. The Galilean satellites' IAU WG solutions for α_S and δ_S , here denoted α^{IAU} and δ^{IAU} , have the same form as Eq. (53), while the rotation angle W , here denoted W^{IAU} , is expressed as Eqs. (54), see Table 11. The arguments of the periodic terms are listed as J_j with $j = 3, \dots, 8$. The mean values for α^{IAU} and δ^{IAU} , which correspond to the Laplace plane coordinates, are similar for the four satellites, whereas their linear terms are identical.

Since its very first report [Davies et al., 1980], the WGCCRE has openly assumed that the North pole of rotation of the Galilean satellites lies along the normal to their orbit, neglecting their small orbital obliquities in the expression for α^{IAU} and δ^{IAU} . They also neglect the mean longitude variations and small librations in the periodic series of W^{IAU} . It can be indeed verified numerically that in the IAU WG solution, ΔW consists

	Cst (°)	Linear term (°)	J_3	J_4	J_5	J_6	J_7	J_8
Period (y)			7.4216	30.2191	137.3522	559.8756	15.1095	5.9308
f_j (rad/y)			0.84661	0.20792	0.045745	0.011222	0.41584	1.0594
f_j (°/cent.)			4850.7	1191.3	262.1	64.3	2382.6	6070.0
φ_j (°)			283.90	355.80	119.90	229.80	352.25	113.35
Io								
α^{IAU}	268.05	$-0.009 T$	0.094	0.024	—	—	—	—
δ^{IAU}	64.50	$0.003 T$	0.040	0.011	—	—	—	—
W^{IAU}	200.39	$203.4889538 d$	-0.085	-0.022	—	—	—	—
Europa								
α^{IAU}	268.08	$-0.009 T$	—	1.086	0.060	0.015	0.009	—
δ^{IAU}	64.51	$0.003 T$	—	0.468	0.026	0.007	0.002	—
W^{IAU}	36.022	$101.3747235 d$	—	-0.980	-0.054	-0.014	-0.008	—
Ganymede								
α^{IAU}	268.20	$-0.009 T$	—	-0.037	0.431	0.091	—	—
δ^{IAU}	64.57	$0.003 T$	—	-0.016	0.186	0.039	—	—
W^{IAU}	44.064	$50.3176081 d$	—	0.033	-0.389	-0.082	—	—
Callisto								
α^{IAU}	268.72	$-0.009 T$	—	—	-0.068	0.590	—	0.010
δ^{IAU}	64.83	$0.003 T$	—	—	-0.029	0.254	—	-0.004
W^{IAU}	259.51	$21.5710715 d$	—	—	0.061	-0.533	—	-0.009

Table 11: Rotation model of the IAU WGCCRE for the four Galilean satellites [Archinal et al., 2018]. The IAU WG arguments J_j are expressed in the form $f_j T + \varphi_j$ in Eqs. (53-54), with f_j and φ_j the frequency and phase, respectively. α^{IAU} and W^{IAU} are expressed as sine series whereas δ^{IAU} is expressed as a cosine series. The amplitudes are given in degrees and T (d) is the time in Julian centuries (days) from J2000.

only in $\Delta\mu$, a projection of the $\Delta\alpha$ series, and assumes $\gamma_u = \Delta\mathcal{L} + \gamma_f = 0$, see Eqs. (23e and 33). In addition to neglecting orbital obliquity and librations, the IAU WG model is also outdated. In particular, the periodic series based on Lieske ephemerides [Lieske, 1979] have remained unchanged ever since.

Pending an actual measurement of orientation and rotation angles, and with some simplifications as detailed below, the solution obtained in Section 6.3 above assuming that the Galilean satellites are entirely solid and are locked in the multi-frequency Cassini state with non-zero obliquities and considering a recent orbital theory would be a perfectly acceptable replacement of the current IAU WG solution. The only thing we do not calculate here is the value of the libration γ_u . Libration computations can be found in Rambaux et al. [2011] or Van Hoolst et al. [2013]. The periodic variations $\Delta\mu$ that are included in the rotation angle W are the periodic terms of the transformation from $\phi_{Inertial}$, see Eq. (34), and therefore does not include γ_u .

The Earth equatorial coordinates α_{LP} and δ_{LP} of the Laplace planes of our solution are close to those of the IAU WG solutions (they differ at most by 0.01° and 0.005° , respectively), but more precise, see Table 1. We therefore recommend updating the mean values of α^{IAU} and δ^{IAU} with α_{LP} and $\delta_{LP} + \delta_{S0}$ as given in Tables 1 and 3, using at least three digits after the decimal point to take advantage of the improved precision achieved by recent ephemerides. The mean value for δ should also include the small increment δ_{S0} , see Eq. (53b), because of the power reduction of a squared sine term in the second-order part of Eq. (8b). Computing a new independent W_0 requires control network computations which are beyond the scope of the present study. Here, the numerical value of W_0 is chosen to ensure that our defined prime meridian location ($W + \alpha_S \sin \delta_S$, where the $\alpha \sin \delta$ term accounts for the equator precession) matches that of the IAU WG model at the J2000 epoch. The corresponding corrections are -0.25 , 2.8 , -4.6 , and -11.5 km, respectively.

The IAU WG rates in α^{IAU} ($-9 \cdot 10^{-5}$ deg/y) and δ^{IAU} ($3 \cdot 10^{-5}$ deg/y) were last updated to match those of Jupiter in the 2005 report [Seidelmann et al., 2007]. Here, with the JUP387 ephemerides, we find rates in α_S and δ_S (e.g. $-6.5 \cdot 10^{-5}$ deg/y and $2.4 \cdot 10^{-5}$ deg/y for Io, see Table 3) that are in good agreement with the rates in Jupiter's equatorial coordinates of the current IAU WG solution ($-6.499 \cdot 10^{-5}$ deg/y and $2.413 \cdot 10^{-5}$

	Cst (°)	Linear term (°)	\mathcal{J}_3	\mathcal{J}_4	\mathcal{J}_5	\mathcal{J}_6	\mathcal{J}_7	\mathcal{J}_8	\mathcal{J}_9
Period (y)			Ω_1	Ω_2	Ω_3	Ω_3	Ω_4	Ω_4	$-2\nu - \Omega_2$
f_j (rad/y)			-7.4217	-30.200	-137.34	-137.34	-561.00	-561.00	-0.68144
f_j (°/cent.)			-0.84660	-0.20805	-0.04575	-0.04575	-0.01120	-0.01120	-9.22041
φ_j (°)			-4850.7	-1192.0	-262.13	-262.13	-64.171	-64.171	-52829.1
			260.604	184.073	59.659	59.182	309.668	310.157	273.914
Io									
α_S	268.0594	-0.0065 T	0.0878	0.0233	0.0030	-	-0.0008	-	0.0023
δ_S	64.4968	0.0024 T	-0.0378	-0.0100	-0.0013	-	0.0003	-	-0.0010
$W - \gamma_u$	200.3980	203.488958424 d	-0.0793	-0.0210	-0.0027	-	0.0007	-	-0.0021
Europa									
α_S	268.0850	-0.0065 T	-0.0049	1.2097	0.0595	-	0.0131	-	0.0007
δ_S	64.5070	0.0024 T	0.0021	-0.5206	-0.0256	-	-0.0056	-	-0.0003
$W - \gamma_u$	35.9172	101.374724491 d	0.0044	-1.0920	-0.0537	-	-0.0118	-	-0.0007
Ganymede									
α_S	268.2044	-0.0065 T	-	-0.1132	0.5066	-	-	0.0922	-
δ_S	64.5678	0.0024 T	-	0.0486	-0.2176	-	-	-0.0396	-
$W - \gamma_u$	44.1652	50.317607524 d	-	0.1022	-0.4575	-	-	-0.0833	-
Callisto									
α_S	268.7322	-0.0065 T	-	-	-	0.1470	0.9253	-	-
δ_S	64.8229	0.0024 T	-	-	-	-0.0626	-0.3936	-	-
$W - \gamma_u$	259.7839	21.571072373 d	-	-	-	-0.1331	-0.8374	-	-
			\mathcal{J}_{10}	\mathcal{J}_{11}	\mathcal{J}_{12}	\mathcal{J}_{13}	\mathcal{J}_{14}	\mathcal{J}_{15}	\mathcal{J}_{16}
Period (y)			$2L_S$	$2\Omega_2$	$-L_S$	$\Omega_2 + \Omega_3$	$2\Omega_3$	$\Omega_3 + \Omega_4$	$2\Omega_4$
f_j (rad/y)			5.9312	-15.101	-11.863	-24.756	-68.661	-110.31	-280.37
f_j (°/cent.)			1.05934	-0.41609	-0.52963	-0.25380	-0.09151	-0.05696	-0.02241
φ_j (°)			6069.6	-2384.0	-3034.6	-1454.2	-524.31	-326.36	-128.40
			113.500	8.146	298.879	243.626	119.318	8.850	259.337
Io									
α_S			-	-	-	-	-	-	-
δ_S			-	-	-	-	-	-	-
$W - \gamma_u$			-	-	-	-	-	-	-
Europa									
α_S			0.0013	-0.0115	0.0007	-0.0011	-	-	-
δ_S			-0.0005	0.0025	-0.0003	0.0002	-	-	-
$W - \gamma_u$			-0.0011	0.0116	-0.0006	0.0011	-	-	-
Ganymede									
α_S			0.0010	-	-0.0010	0.0009	-0.0020	-	-
δ_S			-0.0004	-	0.0004	-0.0002	0.0004	-	-
$W - \gamma_u$			-0.0009	-	0.0009	-0.0009	0.0020	-	-
Callisto									
α_S			-	-	-	-	-	-0.0022	-0.0068
δ_S			-	-	-	-	-	0.0005	0.0014
$W - \gamma_u$			-	-	-	-	-	0.0022	0.0068

Table 12: Proposed update for the solution (α_S , δ_S and W) of the Galilean satellites considered as entirely rigid and using the JUP387 orbital theory, with a limited number of terms (5, 9, 7, and 4, respectively) and a limited set of arguments (14). The arguments \mathcal{J}_j are expressed in the form $f_j T + \varphi_j$ in Eqs. (53-54), with f_j and φ_j the frequency and phase, respectively. α_S and W_S are expressed as sine series whereas δ_S is expressed as a cosine series. The amplitudes are given in degrees and T (d) is the time in Julian centuries (days) from J2000. The column header shows the identification to the fundamental arguments, using the reduced set of arguments \mathcal{J}_j , whose physical origin is recalled on the first line. Compared to the full solution of Table 9 for the periodic terms, the precision is degraded to about 0.001° . Our model does not include any physical libration ($\gamma_u = 0$).

deg/y). We therefore recommend updating the α and δ IAU WG rates for the Galilean satellites to the currently adopted rate for Jupiter. For the rates in W , those of Table 3, based on recent ephemerides, could replace the IAU WG rates.

Each term in the periodic series of the IAU WG (α, δ, W) solution can be replaced by the equivalent term

of our solution for a solid satellite, see Table 9, which has (almost) the same period as the IAU WG term, but a different amplitude, which, as we will see later, ultimately leads to the neglect of one of the replaced terms (the term for Callisto at period 5.93 years). Thanks to the use of more recent and precise ephemeris, the second-order part of the transformation to α and δ , and the non-zero obliquity, we find several additional terms that can be considered for an update of the IAU WG model, depending on the precision required. For Callisto, three of these additional terms have amplitudes larger than the sixth term of the series, which corresponds to the third term of the IAU WG series (the very one we will be neglecting below). Note that when considering different interior structures for a satellite with a global ocean (see for example section 8.2), some amplitudes may be significantly different from their solid counterparts if the forcing frequency is close enough to one of the free mode frequencies, so that the order of the different terms may differ.

The IAU WG arguments are characterized by positive rates while in our solution (Table 9), the rates of the arguments are mostly negative, which makes more sense from a dynamic point of view. Throughout our successive developments, from ephemerides to $\Delta\alpha_S$, $\Delta\delta_S$ and $\Delta\mu$ series, we have kept, at least for the first-order terms of the transformation, signs of rates that correspond to the convention used for the periodic series of Eq. (48) for $n_{x/y}$, where a retrograde precession of the orbital node is characterized by a negative rate. This convention allows for the use of the dynamical Eq. (13) with $\dot{\Omega} = f_j$ to get the amplitudes (Eq. 49) of the periodic series of Eq. (50) for $s_{x/y}$. In this way, we can easily compare the forced frequencies f_j with the κ/C free frequency to identify the potential for resonant amplification. With this convention, the phases remain unchanged by the transformation from $\Delta s_x/\Delta s_y$ to $\Delta\alpha_S/\Delta\delta_S/\Delta\mu$ and, as a result, differ from those of the IAU WG arguments, while the different terms of $\Delta\alpha_S$ and $\Delta\delta_S$ have amplitude of opposite signs for the same argument, when the signs are the same in the IAU WG series.

The current IAU WG solution includes a limited number of terms and is provided with a presumed accuracy of 0.01° on each nutation amplitudes (we assumed the precision is one order higher than the given number of digits). Our solution is by construction more accurate (to within about 0.001° degrees for the time-series in α , due to the truncation error of Table 9), but is based on the assumption that the satellites are entirely rigid. Therefore, it is not certain that, for the time being, an update of the IAU WG solution should include as many terms as ours. If a simplified model with an accuracy of the order of 0.001° on each nutation term is considered sufficient for the four satellites, some simplifications can be made to the periodic series of Table 9. Firstly, we propose to retain only the 5, 9, 7, and 4 largest terms, respectively, for the four satellites. Thus, the 5.93-year periodicity reported for Callisto in Archinal et al. [2018] and also observed in Table 4 (third line) is neglected here (its period is much shorter than the free precession period of approximately 204 years, so that the associated inertial obliquity amplitude is significantly smaller than the inclination amplitude). Next, we suggest reducing the number of arguments used to express the solution. Remember that some arguments listed in Table 9 correspond to identical combinations of fundamental frequencies but may differ slightly in value between satellites due to fitting to numerical integrations (e.g., $\dot{\Omega}_4 = -0.01113$ rad/year in the Io series, versus -0.01120 rad/year in the Callisto series). When such differences do not degrade the model's accuracy beyond the 0.0005° -degree threshold, we use a common value for the argument across satellites. For example, for Ω_1 , which dominates the periodic series of Io, but is only fifth in the series for Europa, we choose the value of the argument as found Io's series, see Table 12. The differences from the original arguments are usually smaller than 10^{-4} rad/year and 0.5° in frequency and phase, respectively. Only differences in phase value can cause differences in the time domain that exceed the threshold. The precision of the time series obtained using 14 different arguments rather than the 25 arguments of Table 9 is smaller than 0.0002° . The proposed update for the IAU WG solution, with the simplified periodic series, is given in Table 12. There is no physical libration in the expression for W , only periodic variations due to the projection of the spin precession/nutations. The differences between our model based on the JUP orbital theory and the IAU WG solution of Archinal et al. [2018] can reach up to 0.4° after 100 years, see Fig. 9.

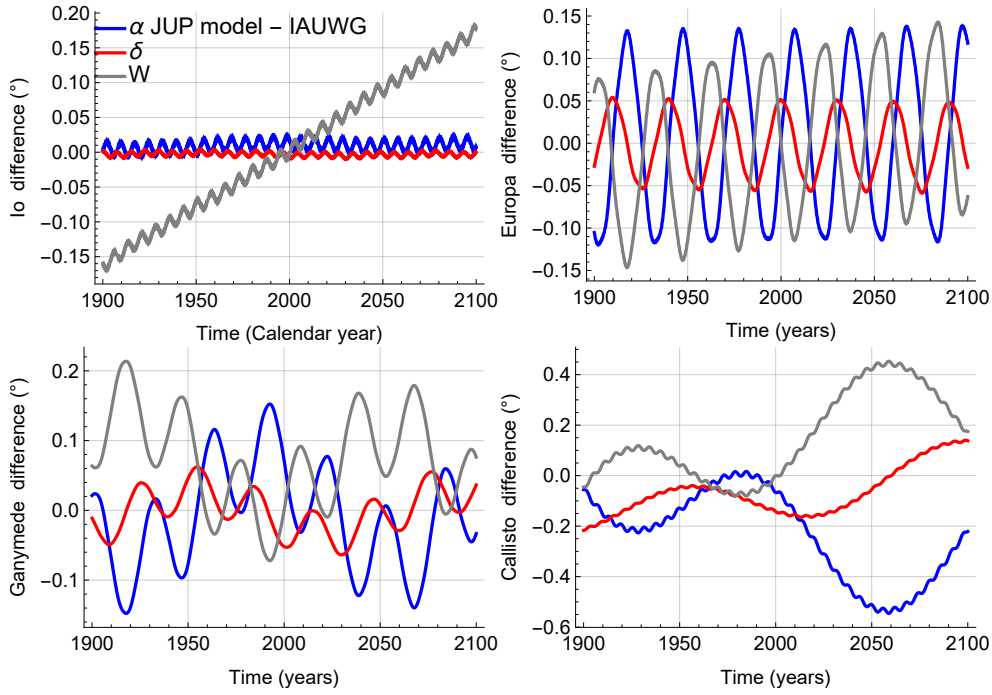


Figure 9: Differences in right ascension, declination, and rotation angle between our model and the IAU WG solution [Archinal et al., 2018] for each of the four Galilean satellites.

8 Discussion

8.1 Sensitivity to the choice of ephemeris

	Io	Europa	Ganymede	Callisto
Laplace pole:				
α_{LP} ($^{\circ}$)	268.0590 (+0.0004)	268.0850 (+0.0001)	268.2049 (-0.0005)	268.7352 (-0.0030)
δ_{LP} ($^{\circ}$)	64.4970 (-0.0002)	64.5093 (+0.0002)	64.5668 (0.0015)	64.8203 (+0.0041)
Transformation coefficients:				
$1 / \cos \delta_{LP}$	2.3226	2.3236	2.3285	2.3504
$\tan \delta_{LP} / \cos \delta_{LP}$	4.8687	4.8736	4.8965	4.9995
$-1/2 \tan \delta_{LP}$	-1.0481	-1.0487	-1.0514	-1.0635
$\cos \delta_{LP}$	0.4306	0.4304	0.4295	0.4255
$-\sin \delta_{LP}$	-0.9026	-0.9027	-0.9031	-0.9050
$1/4 \sin 2\delta_{LP}$	0.1943	0.1942	0.1939	0.1925

Table 13: Numerical values for the orientation angles of the Laplace plane for the four Galilean satellites and transformation coefficients, using the NOE ephemerides. The values in parentheses for α_{LP} and δ_{LP} indicate the increments needed to obtain the JUP387 values, see Table 1.

A comparison between the orbit orientations of the Galilean satellites obtained with JUP387 or NOE reveals differences, on both short and long time scales, see Fig. 10. As with JUP387, we numerically fit the Laplace plane coordinates $(\alpha_{LP}, \delta_{LP})$, a periodic series and one secular term for the projected coordinates (n_x, n_y) of the orbit normal onto the Laplace plane. The Laplace plane coordinates differ by as much as 0.004° from those associated to JUP387, which also affects some of the transformation coefficients, see Table 13. The small secular rates ($tr_{x/y}$) associated to the two ephemerides differ significantly, see Tables 3 and 15, with discrepancies in $n_{x/y}$ reaching up to 0.005° after 100 years, corresponding to a difference up to

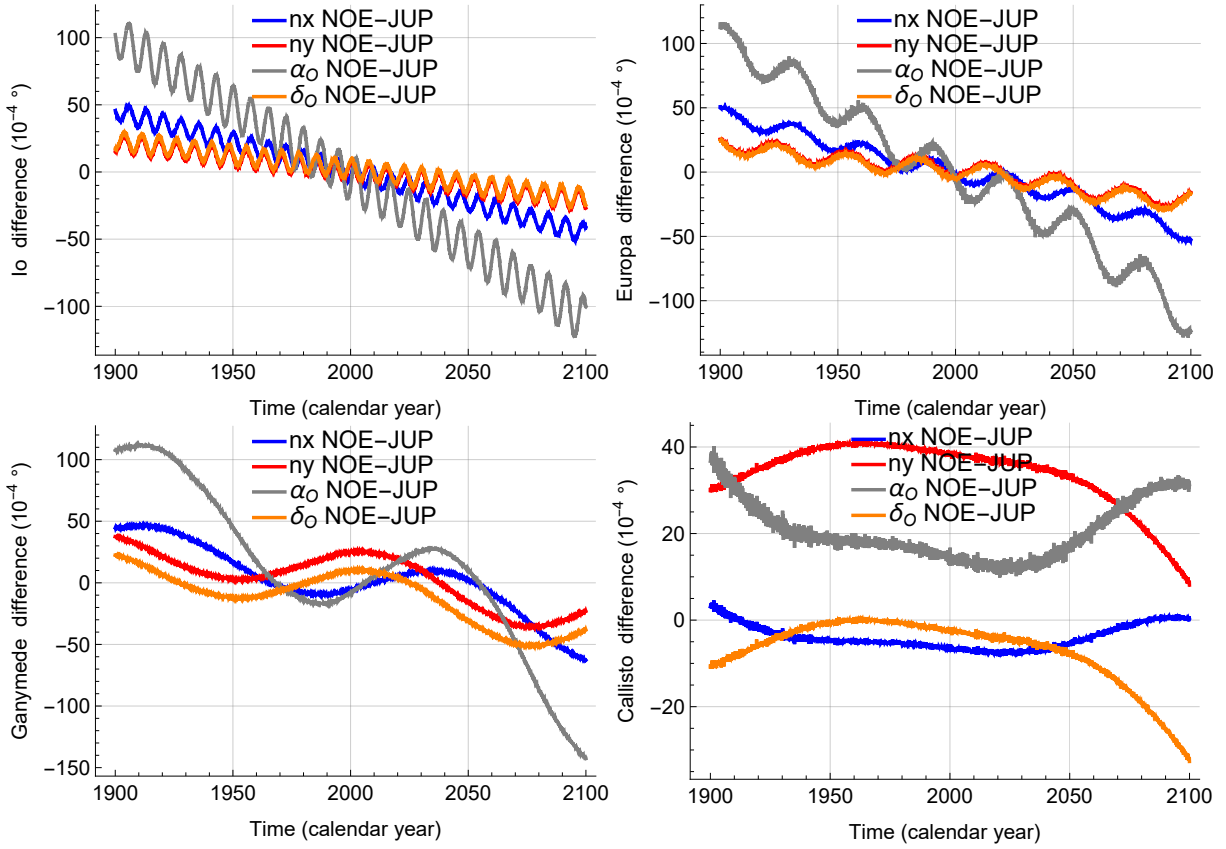


Figure 10: Differences in orbit coordinates $n_{x,y}$ and orbital right ascension α_O and declination δ_O between the JUP387 and NOE ephemerides as a function of time, for the four Galilean satellites.

150 km in the position of the Galilean satellite around Jupiter. The differences in the amplitudes of the $n_{x/y}$ series between JUP387 and NOE range from approximately $3 \cdot 10^{-4}$ deg (for Io) to $2 \cdot 10^{-3}$ deg (for Callisto), see Tables 4 and 14. Note that for each satellite, since the Laplace planes of JUP387 and NOE are different, the $n_{x/y}$ coordinates corresponding to each ephemerides are expressed in a different reference frame. The transformation into equatorial coordinates α_O and δ_O allows for a comparison of the orbit orientation in an identical reference frame (see gray and orange curves in Fig. 10).

As we did with the JUP387 orbital theory, we compute the values of the amplitudes ε_j and θ_j considering a solid interior model, see Table 14, to obtain the complete (s_x, s_y) solution. Then we transform the latter into solutions for the equatorial coordinates α_S, δ_S and μ , including rates, see Table 15, and periodic terms, see Table 16. We applied the same level of truncation as in Table 4, and obtained the same number of terms for Europa, Ganymede and Callisto as with the JUP387 theory, but one more term for Io. By applying similar simplifications as in Section 7 for the solution derived from the JUP387 theory, we propose an alternative update for the IAU WG solution, but based on the NOE orbital theory, see Table 17. For the α and δ rates, we have retained the values derived from the fit of the orbital precession of the NOE orbital theory, which are quite different from the values we recommend for a replacement of the IAU WG solution based on the JUP387 orbital theory.

Figure 11 shows the orbit normal and spin motion of Europa in the ICRF plane over a 9-year period. The angular separation between the spin axis and the orbit normal (also referred to as the orbital obliquity) is clearly noticeable. The spin motion is shown for both a solid interior model and an interior model with an internal global liquid ocean (see discussion in Section 8.2). The difference between the JUP and NOE models is not noticeable at this scale. As expected, the IAU WG model remains close to the orbit normal path, but deviates significantly from the spin axis trajectory. For reference, the solutions of Bills and Scott [2022] for the orbit normal and spin motion, which are inconsistent with both the IAU WG model and our solutions, are also shown in the figure.

	i_j (°)	ε_j (°)	θ_j (°)	period (y)	f_j (rad/y)	φ_j (°)	Argument	\dot{J}_{IAU}
Io								
1	0.0361	0.0020	0.0382	-7.42169	-0.84660	259.686	Ω_1	$-\dot{J}_3$
2	0.0099	0.0001	0.0100	-30.2013	-0.20804	184.127	Ω_2	$-\dot{J}_4$
3	0.0013	0.0000	0.0013	-137.748	-0.04561	60.350	Ω_3	$-\dot{J}_5$
4	0.0004	0.0006	0.0010	-0.68144	-9.22041	273.900	$-2\nu - \Omega_2$	
5	-0.0003	0.0000	-0.0003	-557.341	-0.01127	312.374	Ω_4	$-\dot{J}_6$
6	0.0003	0.0000	0.0003	5.93112	1.05936	113.576	$2L_S$	\dot{J}_8
7	-0.0001	0.0000	-0.0001	-11.8632	-0.52963	298.256	$-L_S$	$-\dot{J}_8/2$
Europa								
1	0.4645	0.0554	0.5200	-30.2013	-0.208084	184.097	Ω_2	$-\dot{J}_4$
2	0.0249	0.0006	0.0254	-137.543	-0.04568	60.120	Ω_3	$-\dot{J}_5$
3	0.0055	0.0000	0.0055	-560.525	-0.01121	309.300	Ω_4	$-\dot{J}_6$
4	-0.0012	-0.0009	-0.0021	-7.42169	-0.84660	259.662	Ω_1	$-\dot{J}_3$
5	-0.0012	0.0015	0.0003	-0.68144	-9.22041	273.890	$-2\nu - \Omega_2$	
6	0.0008	0.0003	0.0005	5.93117	1.05935	113.503	$2L_S$	\dot{J}_8
7	0.0002	-0.0002	0.0000	-0.66965	-9.38278	37.839	$-2\nu - \Omega_3$	
8	0.0002	0.0001	0.0003	-11.8636	-0.52962	299.287	$-L_S$	$-\dot{J}_8/2$
9	-0.0001	0.0000	-0.0001	4.9576	1.26738	68.087	$2L_S - \Omega_2 + \Omega_0$	
Ganymede								
1	0.1845	0.0313	0.2158	-137.532	-0.04569	59.999	Ω_3	$-\dot{J}_5$
2	0.0376	0.0014	0.0390	-560.304	-0.01121	309.329	Ω_4	$-\dot{J}_6$
3	-0.0165	-0.0320	-0.0485	-30.2014	-0.20804	183.990	Ω_2	$-\dot{J}_4$
4	0.0018	-0.0014	0.0004	5.93126	1.05933	113.428	$2L_S$	\dot{J}_8
5	0.0003	-0.0007	-0.0004	-11.8629	-0.52965	298.928	$-L_S$	$-\dot{J}_8/2$
6	0.0002	-0.0002	0.0000	-0.68144	-9.22041	273.804	$-2\nu - \Omega_2$	
7	0.0002	-0.0002	0.0000	3.95426	1.58897	132.963	$3L_S$	$3\dot{J}_8/2$
8	0.0002	-0.0001	0.0001	11.8637	0.52961	178.089	L_S	$\dot{J}_8/2$
9	-0.0001	0.0001	0.0000	5.6858	1.10507	191.565	$2L_S - 2\Omega_3 + \Omega_0$	
Callisto								
1	0.2486	0.1421	0.3907	-559.98	-0.01122	308.856	Ω_4	$-\dot{J}_6$
2	-0.0301	0.0927	0.0626	-137.535	-0.04568	59.519	Ω_3	$-\dot{J}_5$
3	0.0038	-0.0037	0.0001	5.93109	1.05936	112.748	$2L_S$	\dot{J}_8
4	-0.0006	0.0007	0.0001	-30.2024	-0.20804	183.563	Ω_2	$-\dot{J}_4$
5	0.0006	-0.0006	0.0000	-11.8638	-0.52961	298.699	$-L_S$	$-\dot{J}_8/2$
6	0.0005	-0.0005	0.0000	11.8645	0.52958	177.598	L_S	$\dot{J}_8/2$
7	0.0004	-0.0004	0.0000	3.9543	1.58895	132.474	$3L_S$	$3\dot{J}_8/2$
8	-0.0003	0.0003	0.0000	5.86882	1.07060	302.232	$2L_S - \Omega_4 + \Omega_0$	

Table 14: Inclination, orbital and inertial obliquity amplitudes i_j , ε_j and θ_j at the frequency and phase f_j and φ_j obtained from the NOE orbital theory and assuming that the satellites are entirely solid and rigid. The phases φ_j are given with respect to J2000 epoch. The last columns show the identification to the fundamental arguments of Lainey et al. [2006] and the fundamental IAU WG frequencies \dot{J}_i .

	tr_x (°/y)	$tr_y = tr_\delta$ (°/y)	tr_α (°/y)	tr_μ (°/y)	\dot{W} (°/d)	δ_{S0} (°)
Io	$-7.3 \cdot 10^{-5}$	$2.8 \cdot 10^{-6}$	$-1.7 \cdot 10^{-4}$	$1.5 \cdot 10^{-4}$	203.4889584317	$-1.4 \cdot 10^{-4}$
Europa	$-7.3 \cdot 10^{-5}$	$3.0 \cdot 10^{-6}$	$-1.7 \cdot 10^{-4}$	$1.5 \cdot 10^{-4}$	101.3747246256	$-2.5 \cdot 10^{-3}$
Ganymede	$-7.2 \cdot 10^{-5}$	$4.1 \cdot 10^{-6}$	$-1.7 \cdot 10^{-4}$	$1.5 \cdot 10^{-4}$	50.3176077039	$-4.6 \cdot 10^{-4}$
Callisto	$-6.7 \cdot 10^{-5}$	$8.6 \cdot 10^{-6}$	$-1.6 \cdot 10^{-4}$	$1.4 \cdot 10^{-4}$	21.5710726895	$-1.4 \cdot 10^{-3}$

Table 15: Trends in the various quantities considered, obtained for NOE orbital theory. See Table 3 for more details on the definition of the quantities.

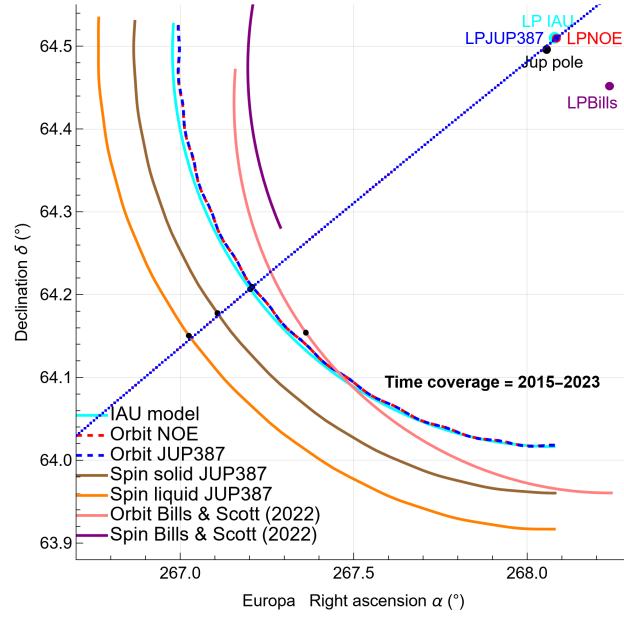


Figure 11: Comparison of the orbit and the spin position (for a solid satellite and one with a liquid layer) in the right ascension/declination plane for Europa. Three orbital theories are compared: JUP387 (blue), NOE (red, below the JUP387 curve), IAU WG model (cyan). The spin position is plotted in a solid case (brown) and a liquid case (orange, obliquity of 0.1 deg). The time range covered by the plot is 2015.5-2023.5. The black dots are evaluated in 2020.0. The instantaneous Cassini plane is also plotted with dotted lines. Different Laplace poles are also shown.

8.2 Effect of the interior model

In the previous sections, the satellites were assumed to be entirely solid. Europa, Ganymede, and Callisto, which are the targets of three future missions or missions currently in cruise phase (JUICE, Europa Clipper, Tianwen-4), are believed to harbor a global internal ocean [e.g. Khurana et al., 1998, Kivelson et al., 2002], however. The presence of a fully molten magma ocean inside Io suggested by (Spohn [1997], Khurana et al. [2011]) has been recently ruled out by the measurement of the satellite’s tidal response (Park et al. [2025]). Although Io most likely has a liquid core (Spohn [1997]), its effect on the satellite’s orientation will not be evaluated here, as the first Galilean satellite is not currently the primary target of any approved space mission, and therefore its rotation will not be observed in the reasonably near future.

We consider a wide range of interior structure models for Europa, Ganymede and Callisto, consistent with known constraints (mass, radius, and MOI), by varying the densities and sizes of their different layers in ranges similar to those of Baland et al. [2012] or Coyette et al. [2025] and use the theoretical angular momentum model of Baland et al. [2019] for a synchronous satellite with an internal global fluid layer to compute the ranges of obliquity amplitudes and build the series for $s_{x/y}$. The series for α , δ , and μ are then obtained with the transformations described in Sections 3 and 4. As anticipated in Section 6.2, the amplitudes of the spin axis motion at a given forcing frequency can differ significantly from the values obtained in the solid case when one of the free frequencies associated with the interior is sufficiently close to the forcing frequency. In such cases, the ordering of the terms may differ from the ordering in the solid case, and the approximation for $\varepsilon(t)$, $\theta(t)$, $\zeta(t)$, and $\psi(t)$ that assume the existence of a dominant amplitude (e.g. Eqs. 51) become ineffective when two amplitudes dominate the solution together. Because of resonant amplification, obliquity amplitudes can reach very large absolute values, which can be considered unrealistic given that tidal damping is not taken into account in the dynamic model. Therefore, we remove the most extreme 5% of values from each range of obliquity amplitudes before calculating the minimum and maximal values from the remaining set. This gives us indicative limits for the obliquity, right ascension, and declination amplitudes, see Table 18, which do not necessarily imply that an amplitude cannot be larger or smaller than these limits.

Typical ranges for the periods of the three modes associated with the precession in space for Ganymede

	α_j^S (°)	δ_j^S (°)	μ_j (°)	period (y)	f_j (rad/y)	φ_j (°)	Argument	\dot{J}_{IAU}
Io								
1	0.0886	-0.0382	-0.0800	-7.42169	-0.8466	259.686	Ω_1	$-\dot{J}_3$
2	0.0233	-0.0100	-0.0210	-30.2013	-0.2080	184.127	Ω_2	$-\dot{J}_4$
3	0.0029	-0.0013	-0.0027	-137.748	-0.0456	60.350	Ω_3	$-\dot{J}_5$
4	0.0023	-0.0010	-0.0020	-0.68144	-9.2204	273.900	$-2\nu - \Omega_2$	
5	-0.0008	0.0003	0.0007	-557.341	-0.0113	312.374	Ω_4	$-\dot{J}_6$
6	0.0006	-0.0003	-0.0005	5.9311	1.0594	113.576	$2L_S$	\dot{J}_8
7	-0.0002	0.0001	0.0002	-11.8632	-0.5296	298.235	$-L_S$	$-\dot{J}_8/2$
Europa								
1	1.2082	-0.5200	-1.0906	-30.2013	-0.2080	184.097	Ω_2	$-\dot{J}_4$
2	0.0591	-0.0254	-0.0534	-137.543	-0.0457	60.1204	Ω_3	$-\dot{J}_5$
3	0.0129	-0.0055	-0.0116	-560.525	-0.0112	309.299	Ω_4	$-\dot{J}_6$
4 (O2)	-0.0115	0.0025	0.0116	-15.1006	-0.4161	8.194	$2\Omega_2$	$-\dot{J}_7 = -2\dot{J}_4$
5	-0.0049	0.0021	0.0044	-7.4269	-0.8466	259.658	Ω_1	$-\dot{J}_3$
6	0.0013	-0.0005	-0.0011	5.93117	1.0594	113.496	$2L_S$	\dot{J}_8
7	0.0007	-0.0003	-0.0007	-0.68144	-9.2204	273.892	$-2\nu - \Omega_2$	
8	0.0007	-0.0003	-0.0006	-11.8636	-0.5296	299.274	$-L_S$	$-\dot{J}_8/2$
9 (O2)	0.0000	-0.0002	0.0000	-38.6985	-0.1624	123.977	$\Omega_2 - \Omega_3$	$-\dot{J}_4 + \dot{J}_5$
10 (O2)	-0.0011	0.0002	0.0011	-24.7637	-0.2537	244.217	$\Omega_2 + \Omega_3$	$-\dot{J}_4 - \dot{J}_5$
Ganymede								
1	0.5025	-0.2158	-0.4538	-137.532	-0.04569	59.999	Ω_3	$-\dot{J}_5$
2	-0.1129	0.0485	0.1019	-30.2014	-0.20804	183.990	Ω_2	$-\dot{J}_4$
3	0.0907	-0.0390	-0.0819	-560.304	-0.01121	309.328	Ω_4	$-\dot{J}_6$
4 (O2)	-0.0020	0.0004	0.0020	-68.766	-0.09137	119.999	$2\Omega_3$	$-2\dot{J}_5$
5	-0.0010	0.0004	0.0009	-11.8629	-0.52965	298.928	$-L_S$	$-\dot{J}_8/2$
6	0.0010	-0.0004	-0.0009	5.93126	1.05933	113.428	$2L_S$	\dot{J}_8
7 (O2)	0.0000	0.0002	0.0000	-38.6997	-0.16236	123.991	$\Omega_2 - \Omega_3$	$-\dot{J}_4 + \dot{J}_5$
8 (O2)	0.0009	-0.0002	-0.0009	-24.7635	-0.25373	243.990	$\Omega_2 + \Omega_3$	$-\dot{J}_4 - \dot{J}_5$
9 (O2)	0.0000	-0.0002	0.0000	182.273	0.03447	249.329	$-\Omega_3 + \Omega_4$	$\dot{J}_5 - \dot{J}_6$
10 (O2)	-0.0007	0.0002	0.0007	-110.427	-0.05690	9.328	$\Omega_3 + \Omega_4$	$-\dot{J}_5 - \dot{J}_6$
Callisto								
1	0.9183	-0.3907	-0.8310	-559.68	-0.01122	308.856	Ω_4	$-\dot{J}_6$
2	0.1473	-0.0626	-0.1333	-137.535	-0.04568	59.519	Ω_3	$-\dot{J}_5$
3 (O2)	-0.0067	0.0014	0.0067	-279.99	0.02244	257.712	$2\Omega_4$	$-2\dot{J}_6$
4 (O2)	0.0000	-0.0005	0.0000	182.312	0.03446	249.337	$-\Omega_3 + \Omega_4$	$\dot{J}_5 - \dot{J}_6$
5 (O2)	-0.0021	0.0005	0.0021	-110.416	0.05690	8.375	$\Omega_3 + \Omega_4$	$-\dot{J}_5 - \dot{J}_6$
6	0.0003	-0.0001	-0.0002	5.93109	1.05936	112.748	$2L_S$	\dot{J}_8

Table 16: Spin position variations $\Delta\alpha_S$, $\Delta\delta_S$ and $\Delta\mu$ for the Galilean satellites for the solid interior model and the NOE orbital theory. The truncation level is 0.0001° . The last columns show the identification to the fundamental frequencies in Lainey et al. [2006] and to the IAU WG frequencies \dot{J}_i . The \dot{J}_i frequencies appearing in Archinal et al. [2018] are indicated in bold. Order 2 terms, not present in the $\Delta s_{x/y}$ series, are labeled with the symbol O2.

and Callisto can be found in Coyette et al. [2025], see their Figs. 8-9. For Europa, the free mode period generally varies between 0 and 0.4 years for the retrograde Free Precession (FP, mode associated with the shell for a satellite with an ocean) and between 3 and 4 years for the retrograde Free Interior Nutation (FIN). The Free Ocean Nutation (FON) can be either prograde or retrograde, with periods ranging from -400 to 400 years. Distinguishing between FON and FIN can be tedious, especially when their periods are similar (Baland et al. [2019] mistakenly reversed them for Titan). We generally note that FIN is the mode in which the period tends to remain larger but close to the period of the FP of the solid case, while the period of FON

	Cst (°)	Linear term (°)	\mathcal{J}_3	\mathcal{J}_4	\mathcal{J}_5	\mathcal{J}_6	\mathcal{J}_7	\mathcal{J}_8	\mathcal{J}_9
			Ω_1	Ω_2	Ω_3	Ω_3	Ω_4	Ω_4	$-2\nu - \Omega_2$
Period (y)			-7.4217	-30.202	-137.49	-137.55	-560.00	-560.50	-0.68144
f_j (rad/y)			-0.84660	-0.20804	-0.0457	-0.04568	-0.01122	-0.01121	-9.2204
f_j (°/cent.)			-4850.7	-1191.8	-261.79	-261.73	-64.286	-64.229	-52829.0
φ_j (°)			259.686	184.097	59.999	59.519	308.856	309.328	273.900
Io									
α_S	268.0590	-0.017 T	0.0886	0.0233	0.0029	-	-0.0008	-	0.0023
δ_S	64.4969	0.00028 T	-0.0382	-0.0100	-0.0013	-	0.0003	-	-0.0010
$W - \gamma_u$	200.3970	203.48895843 d	-0.0800	-0.0210	-0.0027	-	0.0007	-	-0.0020
Europa									
α_S	268.0850	-0.0169 T	-0.0049	1.2082	0.0591	-	-	0.0129	0.0007
δ_S	64.5068	0.0003 T	0.0021	-0.5200	-0.0254	-	-	-0.0055	-0.0003
$W - \gamma_u$	35.9187	101.37472463 d	0.0044	-1.0906	-0.0534	-	-	-0.0116	-0.0007
Ganymede									
α_S	268.2049	-0.0167 T	-	-0.1129	0.5025	-	-	0.0907	-
δ_S	64.5663	0.00041 T	-	0.0485	-0.2158	-	-	-0.0390	-
$W - \gamma_u$	44.1615	50.317607704 d	-	0.1019	-0.4538	-	-	-0.0819	-
Callisto									
α_S	268.7352	-0.0157 T	-	-	-	0.1473	0.9183	-	-
δ_S	64.8188	0.00086 T	-	-	-	-0.0626	-0.3907	-	-
$W - \gamma_u$	259.7765	21.571072689 d	-	-	-	-0.1333	-0.8310	-	-
			\mathcal{J}_{10}	\mathcal{J}_{11}	\mathcal{J}_{12}	\mathcal{J}_{13}	\mathcal{J}_{14}	\mathcal{J}_{15}	\mathcal{J}_{16}
			$2L_S$	$2\Omega_2$	$-L_S$	$\Omega_2 + \Omega_3$	$2\Omega_3$	$\Omega_3 + \Omega_4$	$2\Omega_4$
Period (y)			5.9309	-15.100	-11.863	-24.766	-68.766	-110.42	-280.00
f_j (rad/y)			1.0594	-0.4161	-0.52965	-0.2537	-0.09137	-0.05690	-0.02244
f_j (°/cent.)			6069.9	-2384.1	-3034.7	-1453.6	-523.51	-326.01	-128.57
φ_j (°)			113.496	8.194	298.928	244.217	119.999	8.375	257.712
Io									
α_S			-	-	-	-	-	-	-
δ_S			-	-	-	-	-	-	-
$W - \gamma_u$			-	-	-	-	-	-	-
Europa									
α_S			0.0013	-0.0115	0.0007	-0.0011	-	-	-
δ_S			-0.0005	0.0025	-0.0003	0.0002	-	-	-
$W - \gamma_u$			-0.0011	0.0116	-0.0006	0.0011	-	-	-
Ganymede									
α_S			0.0010	-	-0.0010	0.0009	-0.0020	-0.0007	-
δ_S			-0.0004	-	0.0004	-0.0002	0.0004	0.0002	-
$W - \gamma_u$			-0.0009	-	0.0009	-0.0009	0.0020	0.0007	-
Callisto									
α_S			-	-	-	-	-	-0.0021	-0.0067
δ_S			-	-	-	-	-	0.0005	0.0014
$W - \gamma_u$			-	-	-	-	-	0.0021	0.0067

Table 17: IAU WG solution (α_S , δ_S and W) of the Galilean satellites considered as entirely rigid and using the NOE orbital theory, with a limited number of terms (5, 9, 8, and 4, respectively) and a limited set of arguments (14). The amplitudes are given in degrees. The column header shows the identification to the fundamental arguments, using the reduced set of arguments \mathcal{J}_i , whose physical origin is recalled on the first line. Compared to the full solution of Table 16 for the periodic terms, the precision is degraded to about 0.001° . Our model does not include any physical libration ($\gamma_u = 0$).

	period (y)	f_j (rad/y)	φ_j (°)	Argument	Range ε_j (°)	Range α_j^S (°)	Range δ_j^S (°)
Europa							
1	-30.2008	-0.20805	184.073	Ω_2	-0.035, 0.2	1.0, 1.5	-0.7, -0.4
4 (O2)	-15.1004	-0.41609	8.146	$2\Omega_2$	-	-0.019, -0.008	0.002, 0.004
Ganymede							
1	-137.328	-0.04575	59.659	Ω_3	0.01, 0.07	0.5, 0.6	-0.3, -0.2
2	-30.2009	-0.20805	183.966	Ω_2	-0.4, 0.8	-1.0, 2.0	-0.8, 0.4
8 (O2)	-24.7565	-0.25380	243.626	$\Omega_2 + \Omega_3$	-	-0.02, 0.008	-0.002, 0.003
Callisto							
1	-560.826	-0.0112	309.668	Ω_4	-0.02, 0.14	0.5, 0.9	-0.4, -0.2
2	-137.327	-0.0458	59.182	Ω_3	0.02, 0.08	-0.02, 0.12	-0.05, 0.007
3 (O2)	-280.413	-0.0224	259.337	$2\Omega_4$	-	-0.007, -0.002	0.005, 0.0014

Table 18: Amplitudes ε_j , α_j^S and δ_j^S for Europa, Ganymede and Callisto for a range of interior models with a liquid layer for the JUP387 orbital theory, after removing the most extreme 5% of values from each range. Only ranges whose limits are relatively far from the solid value and of the order of at least about 0.01 degrees are kept here. The ranges in μ_j can be approximately estimated by scaling the α_j^S column by a factor of -0.9 . For Europa and Callisto, the ranges in corrective term δ_{S0} are also affected by the resonances and are equal to the ranges in the amplitudes δ_4^S and δ_3^S , respectively, of the term with twice the main frequency (order 2 term).

tends to vary within a wider range that may even include negative signs (free prograde motion), see also Baland et al. [2025] for the Uranian satellites.

In Table 18, we present the amplitude ranges whose limits are relatively far from the solid value and of the order of at least about 0.01 degrees. With the exception of the second term of Ganymede, which is amplified by resonance with the FIN, all first-order terms presented are amplified by resonance with the FON. For Europa, ε_1 can be positive (up to about 0.2° when the most extreme values are discarded), but also negative (up to -0.035°), or even close to 0 and therefore deviate considerably from the solid value (0.0555°). The corresponding ranges in α_1 and δ_1 are also widened by the resonance with the FON. Fig. 11 shows an example of how a change in interior model from solid (brown line) to liquid (orange line) affects the spin position in the α, δ plane. The ranges in α_4 and δ_4 of the 15-years second-order term, which is a byproduct of the transformation of the first term in the $s_{x/y}$ series, is also affected by the resonance with the FON. For Ganymede and Callisto, the resonances also significantly widen the ranges of some of the second-order terms (the eighth and third terms, respectively).

9 Conclusions and discussion

This paper presents a method to construct an updated orientation and rotation model for the Galilean satellites. After introducing the different reference frames and set of angles involved in the problem (Section 2), we develop in Section 3 a theoretical framework to accurately transform the spin axis Cartesian coordinates into the declination and right ascension of the spin axis in the ICRF, while minimizing conversion errors. When a target precision of the order of the arcsecond is required, as expected from the JUICE mission measurements, second-order terms must be included in the analytical transformation. We also show how the expressions for the inertial obliquity, node longitude, orbital obliquity, and offset relative to the Cassini plane can be obtained from both the spin axis Cartesian or equatorial coordinates.

Section 4 describes the transformation equations for the rotation angles. ϕ_{Euler} and W are measured along the satellite's equator from the Laplace plane and the ICRF equatorial plane, respectively. However, for the purposes of libration modeling and future measurement interpretation, a third angle which we denote $\phi_{Inertial}$ is used, and is measured from an inertial point on the ICRF equator to the meridian on the satellite's equator. The transformation between W and $\phi_{Inertial}$, denoted μ , is described in Section 4.3. Although we do not solve them in this study, we provide the dynamical equations for the librations, see Section 5.2, in the hope of clarifying the different ways in which librations, and thus the periodic parts of the rotation angle

W , could be calculated.

The proposed analytical second-order transformation method relies solely on spherical trigonometry and is therefore applicable regardless of the adopted dynamical model for the spin precession. If the spin axis Cartesian coordinates are expressed as trigonometric series, the transformed angles preserve this trigonometric form. The other advantages of this method are that the geophysically relevant parameters and the amplitudes of the output series can be readily connected, while error tracing is possible, enabling controlled accuracy. Additionally, the first order transformation coefficients can be used to propagate errors between the different coordinate sets.

Based on the dynamical model described in Section 5, we generate trigonometric series in spin axis Cartesian coordinates. As no direct observations of the Galilean satellites' spin positions are yet available, we adopted as an example a rigid and solid model consistent with the most recent gravity field coefficients, see section 6.1. The series are provided with a truncation level of about 0.0001° . If one obliquity amplitude in the spin axis Cartesian coordinates series is dominant (e.g., for a solid Europa), approximate trigonometric representations can be derived for the inertial and orbital obliquities, node longitude, and offset relative to the Cassini plane (Section 6.2). Frequency combinations (sums and differences of the frequencies of the terms in the spin axis Cartesian coordinates series) naturally appear, leading to new frequencies in Euler angles trigonometric series. The offset can be relatively important. For Europa, the multi-frequency spin position deviates by only 0.005° from the Cassini plane for the solid case, whereas Callisto exhibits the largest offset (up to 0.1°). We converted the spin axis Cartesian coordinates into declination, right ascension, and W series (Section 6.3). Second order terms naturally arise from combinations of either twice the dominant term or two distinct terms, corresponding to the J_7 or J_8 terms in the IAU WG solution.

A solution similar to that of Archinal et al. [2018] can be recovered by reducing the number of frequencies and assuming certain close phases and frequencies to be equal. Our proposed model now includes 14 frequencies shared among the four Galilean satellites, compared to only 6 in the IAU WG model (Section 7). In our solution, frequencies have a sign assigned based on the original frequency in the forcing series (corresponding to prograde or retrograde motions), which is crucial for comparison with the free retrograde mode and for evaluating possible amplifications. The discrepancies between our model and the Lieske [1979] model incorporated in Archinal et al. [2018] can reach up to 0.4° after 100 years. These differences arise from the use of an updated orbital theory and an non-zero obliquity model (whereas the previous IAU WG solution assumed zero obliquity, our model incorporates a theoretical obliquity consistent with a solid, rigid satellite). As in Archinal et al. [2018], our model contains no forced librations in the W series; the periodic variations in W originate solely from the periodic terms of the μ angle.

Our nominal series are based on JUP387, but we also provide equivalent series derived from the NOE ephemerides (Section 8.1). Although the frequencies, phases, and amplitudes differ slightly between the two series, the largest deviations in the spin position are due to the trend differences in the orbital precession. A SPICE kernel for the case of entirely solid satellites has been generated for the α , δ and W angles, using both the JUP and NOE ephemerides. These 2 kernels are currently available on lara.oma.be/GalileanSat/. Another localisation on the SPICE kernel architecture will be available soon. If Europa, Ganymede, or Callisto possess a liquid global ocean beneath the icy shell, certain amplitudes may be amplified, as summarized in Table 18.

We validated our transformation of Sections 3 and 4 by comparing our series of Section 6 with numerical integrations of the full differential equations of motion (Eqs. 42), finding differences smaller than the intrinsic precision of the series. Additional validation was obtained by comparing our Callisto series with those of Noyelles [2009], showing a good agreement in amplitudes. However, we note that the phases reported by Noyelles [2009] appear inconsistent with both Archinal et al. [2018] and our results.

In our computations, the Laplace plane was chosen as the reference plane and consistently with the adopted orbital theory. Each orbital theory defines a slightly different Laplace plane, and various numerical methods and temporal coverages can be employed to determine it. Nevertheless, to first order in small parameters, our multi-frequency theory allows any Laplace plane to be adopted as a reference for frequency decomposition. If we consider Jupiter's equatorial plane instead of the Laplace plane as the reference plane, the resulting differences in spin axis right ascension and declination tend to increase with the tilt of the Laplace plane with respect to Jupiter's equator, and are therefore the largest for Callisto (tilt of 0.43°). This

is because the obliquity relative to this plane becomes larger, making the second-order approximation less appropriate and leading to larger differences in α_S and δ_S . For Io, Europa and Ganymede, the discrepancies reach a few tens of arcseconds 100 years after J2000. For Callisto, considering the equatorial plane of Jupiter instead of the Laplace plane as a reference plane is definitely not recommended (see also Noyelles [2009]).

This study provides a robust foundation for interpretation of future observations of the Galilean satellites' orientation and rotation angles, whether by the JUICE or Europa Clipper spacecraft, or through Earth-based radar measurements. The method can readily be applied to any synchronously rotating satellite whose orbit remains close to its Laplace plane.

Acknowledgment

This work was financially supported by the Belgian PRODEX program managed by the European Space Agency in collaboration with the Belgian Federal Science Policy Office.

We thank Sébastien Le Maistre, Tim Van Hoolst and Valéry Lainey for their helpful comments and discussions. We thank Alfonso Caldiero for testing the SPICE kernel.

References

- J. Anderson, R. Jacobson, E. Lau, W. Moore, and G. Schubert. Io's gravity field and interior structure. *JGR*, 106(E12):32963–32969, 2001.
- B. A. Archinal, C. H. Acton, M. F. A'Hearn, A. Conrad, G. J. Consolmagno, T. Duxbury, D. Hestroffer, J. L. Hilton, R. L. Kirk, S. A. Klioner, D. McCarthy, K. Meech, J. Oberst, J. Ping, P. K. Seidelmann, D. J. Tholen, P. C. Thomas, and I. P. Williams. Report of the IAU Working Group on Cartographic Coordinates and Rotational Elements: 2015. *Celestial Mechanics and Dynamical Astronomy*, 130(3):22, Feb. 2018. doi:10.1007/s10569-017-9805-5.
- R. M. Baland, T. Van Hoolst, M. Yseboodt, and Ö. Karatekin. Titan's obliquity as evidence of a subsurface ocean? *A&A*, 530:A141, 2011.
- R.-M. Baland, M. Yseboodt, and T. Van Hoolst. Obliquity of the Galilean satellites: The influence of a global internal liquid layer. *Icarus*, 220:435–448, 2012.
- R.-M. Baland, M. Yseboodt, and T. Van Hoolst. The obliquity of Enceladus. *Icarus*, 268:12–31, 2016.
- R.-M. Baland, M. Yseboodt, A. Rivoldini, and T. Van Hoolst. Obliquity of Mercury: Influence of the precession of the pericenter and of tides. *Icarus*, 291:136–159, July 2017. doi:10.1016/j.icarus.2017.03.020.
- R.-M. Baland, A. Coyette, and T. Van Hoolst. Coupling between the spin precession and polar motion of a synchronously rotating satellite: application to Titan. *Celestial Mechanics and Dynamical Astronomy*, 131(2):11, Feb. 2019. doi:10.1007/s10569-019-9888-2.
- R.-M. Baland, V. Filice, S. Le Maistre, A. Trinh, M. Yseboodt, and T. Van Hoolst. Librations and obliquity of the largest moons of Uranus. *Icarus*, 426:116371, Jan. 2025. doi:10.1016/j.icarus.2024.116371.
- B. G. Bills. Free and forced obliquities of the Galilean satellites of Jupiter. *Icarus*, 175(1):233–247, May 2005. doi:10.1016/j.icarus.2004.10.028.
- B. G. Bills and F. Nimmo. Rotational dynamics and internal structure of Titan. *Icarus*, 214(1):351–355, July 2011. doi:10.1016/j.icarus.2011.04.028.
- B. G. Bills and B. R. Scott. Rotation models for the Galilean satellites. *Planet. Space Sci.*, 219:105474, Sept. 2022. doi:10.1016/j.pss.2022.105474.
- G. Boué. Cassini states of a rigid body with a liquid core. *Celestial Mechanics and Dynamical Astronomy*, 132(3):21, Apr. 2020. doi:10.1007/s10569-020-09961-9.

- H. Camichel, M. Gentili, and B. Lyot. Observations Planetaires au Pic du Midi, en 1941. *L'Astronomie*, 57: 49–60, Jan. 1943.
- P. Cappuccio, A. Hickey, D. Durante, M. Di Benedetto, L. Iess, F. De Marchi, C. Plainaki, A. Milillo, and A. Mura. Ganymede's gravity, tides and rotational state from JUICE's 3GM experiment simulation. *Planet. Space Sci.*, 187:104902, Aug. 2020. doi:10.1016/j.pss.2020.104902.
- P. Cappuccio, M. Di Benedetto, D. Durante, and L. Iess. Callisto and Europa Gravity Measurements from JUICE 3GM Experiment Simulation. *Planet. Sci. Journal*, 3(8):199, Aug. 2022. doi:10.3847/psj/ac83c4.
- G. Colombo. Cassini's Second and Third Laws. *AJ*, 71:891–896, 1966.
- A. Coyette, T. Van Hoolst, R.-M. Baland, and T. Tokano. Modeling the polar motion of Titan. *Icarus*, 265: 1 – 28, 2016. ISSN 0019-1035. doi:http://dx.doi.org/10.1016/j.icarus.2015.10.015.
- A. Coyette, R.-M. Baland, and T. Van Hoolst. Variations in rotation rate and polar motion of a non-hydrostatic Titan. *Icarus*, 307:83–105, June 2018. doi:10.1016/j.icarus.2018.02.003.
- A. Coyette, R.-M. Baland, and T. V. Hoolst. A second-order angular momentum theory for the Cassini states of large satellites: I. Influence of triaxiality and a subsurface ocean. *Submitted to C.M.D.A.*, 2025.
- M. E. Davies and F. Y. Katayama. Coordinates of features on the Galilean satellites. *Journal of Geophysical Research (Planets)*, 86(A10):8635–8657, Sept. 1981. doi:10.1029/JA086iA10p08635.
- M. E. Davies, V. K. Abalakin, C. A. Cross, R. L. Duncombe, H. Masursky, B. Morando, T. C. Owen, P. K. Seidelmann, A. T. Sinclair, G. A. Wilkins, and Y. S. Tjufflin. Report of the IAU Working Group on Cartographic Coordinates and Rotational Elements of the Planets and Satellites. *Celestial Mechanics*, 22 (3):205–230, Oct. 1980. doi:10.1007/BF01229508.
- M. E. Davies, T. R. Colvin, J. Oberst, W. Zeitler, P. Schuster, G. Neukum, A. S. McEwen, C. B. Phillips, P. C. Thomas, J. Veverka, M. J. S. Belton, and G. Schubert. The Control Networks of the Galilean Satellites and Implications for Global Shape. *Icarus*, 135(1):372–376, Sept. 1998. doi:10.1006/icar.1998.5982.
- A. Dollfus and J. B. Murray. La rotation, la cartographie et la photométrie des satellites de Jupiter. In A. Woszczyk and C. Iwaniszewska, editors, *Exploration of the Planetary System*, volume 65 of *IAU Symposium*, pages 513–525, Jan. 1974.
- L. Gomez Casajus, M. Zannoni, D. Modenini, P. Tortora, F. Nimmo, T. Van Hoolst, D. Buccino, and K. Oudrhiri. Updated Europa gravity field and interior structure from a reanalysis of Galileo tracking data. *Icarus*, 358:114187, 2021. ISSN 0019-1035. doi:https://doi.org/10.1016/j.icarus.2020.114187.
- J. Henrard. The Rotation of Europa. *Celestial Mechanics and Dynamical Astronomy*, 91(1-2):131–149, Jan. 2005. doi:10.1007/s10569-005-3833-2.
- J. Henrard and G. Schwanen. Rotation of Synchronous Satellites: Application to the Galilean Satellites. *Celestial Mechanics and Dynamical Astronomy*, 89(2):181–200, Mar. 2004. doi:10.1023/B:CELE.0000034515.57763.33.
- K. K. Khurana, M. G. Kivelson, D. J. Stevenson, G. Schubert, C. T. Russell, R. J. Walker, and C. Polanskey. Induced magnetic fields as evidence for subsurface oceans in Europa and Callisto. *Nature*, 395(6704): 777–780, Oct. 1998. doi:10.1038/27394.
- K. K. Khurana, X. Jia, M. G. Kivelson, F. Nimmo, G. Schubert, and C. T. Russell. Evidence of a Global Magma Ocean in Io's Interior. *Science*, 332(6034):1186, June 2011. doi:10.1126/science.1201425.
- M. G. Kivelson, K. K. Khurana, and M. Volwerk. The Permanent and Inductive Magnetic Moments of Ganymede. *Icarus*, 157(2):507–522, June 2002. doi:10.1006/icar.2002.6834.

- V. Lainey, L. Duriez, and A. Vienne. Synthetic representation of the Galilean satellites' orbital motions from L1 ephemerides. *A&A*, 456(2):783–788, Sept. 2006. doi:10.1051/0004-6361:20064941.
- V. Lainey, J.-E. Arlot, Ö. Karatekin, and T. van Hoolst. Strong tidal dissipation in Io and Jupiter from astrometric observations. *Nature*, 459(7249):957–959, June 2009. doi:10.1038/nature08108.
- J. H. Lieske. Poles of the Galilean satellites. *A&A*, 75(1-2):158–163, May 1979.
- J.-L. Margot. Spin states of Europa and Ganymede. In *EGU Meeting Abstracts #221*, volume EGU25-14788 of *EGU General Assembly 2025, Vienna, Austria, 27 Apr–2 May 2025*, 2025.
- E. Mazarico, D. Buccino, J. Castillo-Rogez, A. J. Dombard, A. Genova, H. Hussmann, W. S. Kiefer, J. I. Lunine, W. B. McKinnon, F. Nimmo, R. S. Park, J. H. Roberts, D. K. Srinivasan, G. Steinbrügge, P. Tortora, and P. Withers. The Europa Clipper Gravity and Radio Science Investigation. *Space Science Reviews*, 219(4):30, June 2023. doi:10.1007/s11214-023-00972-0.
- C. D. Murray and S. F. Dermott. *Solar System Dynamics*. Cambridge University Press, 2000. doi:10.1017/CBO9781139174817.
- B. Noyelles. Expression of Cassini's third law for Callisto, and theory of its rotation. *Icarus*, 202(1):225–239, July 2009. doi:10.1016/j.icarus.2008.12.015.
- B. Noyelles. Theory of the rotation of Janus and Epimetheus. *Icarus*, 207(2):887–902, June 2010. doi:10.1016/j.icarus.2009.12.034.
- R. S. Park, R. A. Jacobson, L. Gomez Casajus, F. Nimmo, A. I. Ermakov, J. T. Keane, W. B. McKinnon, D. J. Stevenson, R. Akiba, B. Idini, D. R. Buccino, A. Magnanini, M. Parisi, P. Tortora, M. Zannoni, A. Mura, D. Durante, L. Iess, J. E. P. Connerney, S. M. Levin, and S. J. Bolton. Io's tidal response precludes a shallow magma ocean. *Nature*, 638(8049):69–73, Feb. 2025. doi:10.1038/s41586-024-08442-5.
- S. J. Peale. Generalized Cassini's Laws. *AJ*, 74:483, Apr. 1969. doi:10.1086/110825.
- N. Rambaux, T. van Hoolst, and Ö. Karatekin. Librational response of Europa, Ganymede, and Callisto with an ocean for a non-Keplerian orbit. *A&A*, 527:A118, Mar. 2011. doi:10.1051/0004-6361/201015304.
- G. Schubert, J. D. Anderson, T. Spohn, and W. B. McKinnon. *Interior composition, structure and dynamics of the Galilean satellites*, volume 1, pages 281–306. Cambridge University Press, 2004.
- P. K. Seidelmann, B. A. Archinal, M. F. A'hearn, A. Conrad, G. J. Consolmagno, D. Hestroffer, J. L. Hilton, G. A. Krasinsky, G. Neumann, J. Oberst, P. Stooke, E. F. Tedesco, D. J. Tholen, P. C. Thomas, and I. P. Williams. Report of the IAU/IAWG Working Group on cartographic coordinates and rotational elements: 2006. *Celestial Mechanics and Dynamical Astronomy*, 98(3):155–180, July 2007. doi:10.1007/s10569-007-9072-y.
- T. Spohn. Tides of io. In H. Wilhelm, W. Zürn, and H.-G. Wenzel, editors, *Lecture Notes in Earth Sciences, Berlin Springer Verlag*, volume 66, pages 345–377. 1997. doi:10.1007/BFb0011459.
- A. Stark, H. Hussmann, G. Steinbrügge, J. Oberst, and T. Roatsch. Resonant Rotation parameters of the Galilean satellites. In *EGU General Assembly Conference Abstracts*, EGU General Assembly Conference Abstracts, page 10488, Apr. 2018.
- G. Steinbrügge, T. Steinke, R. Thor, A. Stark, and H. Hussmann. Measuring Ganymede's Librations with Laser Altimetry. *Geosciences*, 9(7):320, July 2019. doi:10.3390/geosciences9070320.
- E. P. Turtle, A. S. McEwen, G. W. Patterson, C. M. Ernst, C. M. Elder, K. A. Slack, S. E. Hawkins, J. McDermott, H. Meyer, R. DeMajistre, R. Espiritu, H. Seifert, J. Niewola, M. Bland, M. Becker, J. Centurelli, G. C. Collins, P. Corlies, H. Darlington, I. J. Daubar, C. Derr, C. Detelich, E. Donald, W. Edens, L. Fletcher, C. Gardner, F. Graham, C. J. Hansen, C. Haslebacher, A. G. Hayes, D. Humm, T. A. Hurford,

- R. L. Kirk, N. Kutsop, W. J. Lees, D. Lewis, S. London, A. Magner, M. Mills, A. C. Barr Mlinar, F. Morgan, F. Nimmo, A. Ocasio Milanes, S. Osterman, C. B. Phillips, A. Pommerol, L. Prockter, L. C. Quick, G. Robbins, J. M. Soderblom, B. Stewart, A. Stickle, S. S. Sutton, N. Thomas, I. Torres, O. J. Tucker, R. B. Van Auken, and K. A. Wilk. The Europa Imaging System (EIS) Investigation. *Space Science Reviews*, 220(8):91, Dec. 2024. doi:10.1007/s11214-024-01115-9.
- T. Van Hoolst, N. Rambaux, O. Karatekin, V. Dehant, and A. Rivoldini. The librations, shape, and icy shell of europa. *Icarus*, 195(1):386–399, 2008. ISSN 0019-1035. doi:https://doi.org/10.1016/j.icarus.2007.12.011.
- T. Van Hoolst, R.-M. Baland, and A. Trinh. On the librations and tides of large icy satellites. *Icarus*, 226(1):299–315, Sept. 2013. doi:10.1016/j.icarus.2013.05.036.
- M. Yseboodt and J.-L. Margot. Evolution of Mercury’s obliquity. *Icarus*, 181(2):327–337, Apr. 2006. doi:10.1016/j.icarus.2005.11.024.
- M. Yseboodt and T. Van Hoolst. The long-period forced librations of Titan. In *Complex Planetary Systems, Proceedings of the International Astronomical Union*, volume 310 of *IAU Symposium*, pages 25–28, July 2014. doi:10.1017/S1743921314007741.
- M. Yseboodt, R.-M. Baland, and S. Le Maistre. Mars orientation and rotation angles. *Celestial Mechanics and Dynamical Astronomy*, 135(5):50, Oct. 2023. doi:10.1007/s10569-023-10159-y.